表4　HMG-CoA還元酵素阻害薬の種類と用量・用法

一般名	商品名	性質	用量(1日)・用法
プラバスタチン	メバロチン	水溶性	10 mg(分1～分2)(20 mgまで)
シンバスタチン	リポバス	脂溶性	5 mg(分1)(20 mgまで)
フルバスタチン	ローコール	脂溶性	20～30 mg(分1)(60 mgまで)
アトルバスタチン	リピトール	脂溶性	10 mg(分1)(40 mgまで)
ピタバスタチン	リバロ	脂溶性	2 mg(分1)(4 mgまで)
ロスバスタチン	クレストール	水溶性	2.5 mg(分1)(20 mgまで)

在わが国では，プラバスタチン，シンバスタチン，フルバスタチン，アトルバスタチン，ピタバスタチン，ロスバスタチンが市販されている(**表4**)．プラバスタチン，シンバスタチンは糸状菌由来，フルバスタチン，アトルバスタチン，ピタバスタチン，ロスバスタチンは化学合成により作製されたものである．アトルバスタチン，ピタバスタチン，ロスバスタチンは半減期が長く，LDL-Cの低下活性も強いため，ストロングスタチンまたはスーパースタチンと呼ばれることもある．

スタチンのCADに対する一次予防や二次予防の効果は数々の大規模臨床試験により証明されている．一次予防としてはWOSCOPS，AFCAPS/TexCAPS，ALLHAT-LLT，ASCOT-LLA，二次予防としては4S，CARE，LIPIDなどの報告がある．CADに対して，日本人の絶対リスクが欧米人に比較して低いため，日本人に対するLDL-C低下による一次予防の効果について疑問を持たれることもあったが，わが国の大規模臨床試験であるMEGA studyが報告され，プラバスタチンによる18%のLDL-C低下により33%のCAD発生抑制効果を認め，その意義が明らかになった[4]．

スタチンの副作用は消化器症状，肝機能障害，ミオパチーなどが報告されている．重篤な副作用としては横紋筋融解症が有名であり，クレアチニンキナーゼ(CK)が基準値上限の10倍以上に上昇すること，血中ミオグロビンが上昇することなどから診断される．発症頻度は低いが，スタチンとフィブラート系薬剤との併用や腎機能障害患者に現れやすいので注意が必要である．スタチンの妊婦，妊娠の可能性のある婦人への投与は禁忌である．FDAはスタチンの妊婦への投与を最大禁忌(ランクX)としている．授乳中の場合は，授乳を中止するか，スタチン投与を避けるべきである．乳幼児および小児に対しては安全性は確立していないが，海外では2002年，米国のFDAが8歳以上の小児ヘテロ接合体患者に対するプラバスタチンの適応を認可している．

2) 陰イオン交換樹脂(レジン)：コレスチミド，コレスチラミン

LDL-C値が高値であるIIa型高脂血症が適応になる．副作用などによってスタチン投与が不適切である例や，妊娠の可能性のある女性に対して薬物療法が必要である場合にはレジンが選択される．レジンは，スタチンとの併用にてさらに大きな効果を得ることができる．

レジンは，その分子内にCl^-イオンを持ち，このCl^-イオンが胆汁酸と置換されて胆汁酸吸着効果を持つ．レジンは胆汁酸を吸着したまま糞便中に排泄されるため，胆汁酸の再吸収による腸肝循環を阻害して，コレステロールから胆汁酸への異化を促進する．結果として，体内のコレステロールプールを減少させ，LDL受容体の合成を促進し，LDL-C値の低下を来す．一方，LDL受容体の合成促進と同時に肝臓でのコレステロール合成を促進するために，LDL-C値の低下効果の減弱やトリグリセライド値の増加を来すことがある．

レジンの服用でLDL-C値を12.6%低下させることにより，CAD発症リスクを19%低下，CADによる死亡も24%低下させることができたというエビデンス[5,6]は，薬剤によるLDL-C低下によってCAD発症リスクの軽減が可能であるという最初の報告であり，その後の高脂血症治療薬開発につながる画期的なものであった．

レジンの副作用は腹部膨満感や便秘などの消化器症状が主である．非吸収性であることから，重篤な副作用は認められていない．スタチン，ジギ

タリス，ワルファリン，サイアザイド系薬剤，甲状腺製剤などの併用薬剤を吸着することが報告されており，これらの併用薬剤服用に際しては，服用間隔をあけるなどの指導が必要である．

レジンには，以上の脂質低下作用に加えて，近年，基礎代謝の亢進，血糖降下作用，体重減少作用を示すことが報告されている．レジンの服用により，血液中の胆汁酸の組成が変化して，コール酸が相対的に増加する．このため，細胞内で甲状腺ホルモンT4を活性型のT3に転換する酵素の発現が亢進し，エネルギー代謝亢進につながっている可能性が考えられている[7]．

3) フィブラート系薬剤

高トリグリセライド血症に対して最も効果を有する薬剤である．III型，IIb型高脂血症，メタボリックシンドロームや2型糖尿病に合併する脂質異常症に適応となる．

フィブラート系薬剤はペルオキシソーム増殖剤応答性受容体PPAR-αのリガンドとなって活性化し，脂肪酸のβ酸化亢進，肝臓でのトリグリセライド産生減少，リポ蛋白リパーゼ(LPL)活性の促進によりトリグリセライドの分解亢進，アポ蛋白A-I，A-IIの生成増加などの作用を有し，トリグリセライド値の低下，HDL-C値の増加，small dense LDLの低下作用を認める．その他，フィブラートには肝臓でのコレステロール合成抑制作用，PPAR-γを介したインスリン感受性上昇作用，胆汁へのコレステロール排泄促進作用を有するため，LDL-C値の低下も認める．

フィブラートの大規模臨床試験としては，gemfibrozilを用いたHelsinki Heart Study (HHS)で，CAD一次予防において主要心血管イベントが34%低下を認めたが，総死亡や心血管死亡に有意な差を認めなかった[8]．ベザフィブラートを用いてCAD二次予防における有用性を検討したBezafibrate Infarction Prevention Trial(BIP)では主要心血管イベント，心血管死亡，総死亡ともに有意な差を認めなかった[9]．2型糖尿病患者に対してフェノフィブラートのCADに対する一次予防，二次予防の効果をみたFenofibrate Intervention and Event Lowering in Diabetes(FIELD)でも主要心血管イベント，心血管死亡，総死亡には有意差を認めなかったが，MIリスクは有意に減少した[10]．

フィブラートの副作用はミオパチー，肝機能障害，胆石，胃腸障害などが認められ，特に腎機能障害，高齢者，スタチンとの併用時には重篤な副作用である横紋筋融解症の危険性が高くなる．フィブラートとワルファリンとの併用にて，ワルファリンの作用が増強するため，出血傾向が強くなる可能性があり，十分な注意が必要である．

4) プロブコール

IIa型高脂血症，黄色腫を伴う脂質異常症が適応となる．HDL-C値低下作用を持つため，低HDL-C血症に対する投与は慎重に行うべきである．

プロブコールは，酸化防止薬であるブチル化ヒドロキシトルエン(BHT)が2分子結合した構造を有し，脂溶性であるためリポ蛋白中に取り込まれて強力な抗酸化作用を示し，LDL-C値低下作用も有する．LDL-C値低下作用は，LDLの異化促進や，胆汁へのコレステロール排泄促進が考えられているが，詳細は明らかではない．HDL-C値低下作用はABCA-1の抑制，CETPの活性亢進，SR-B1の活性亢進などによると考えられている．

WHHLウサギでプロブコールによる動脈硬化の予防効果が示されている[11]．PTCA施行後の再狭窄予防効果の報告もされている[12,13]．これらの作用は，脂質低下作用よりは抗酸化作用によるものが大きいと考えられている．大規模臨床試験が行われていないため，その効果については明らかではなく，第一選択にはならない．スタチンに忍容性のない患者や，スタチンのみでは効果が十分でない患者に使用される．

副作用は消化器症状，肝障害，発疹，QT延長症候群やtorsades de pointesなどがあり，特に不整脈の予防のために定期的な心電図の施行が望ましい．

5) 小腸コレステロールトランスポーター阻害薬(エゼチミブ)

エゼチミブは，小腸粘膜に存在するNPC1L1と結合して，食事および胆汁由来のコレステロール吸収を阻害することにより，血中LDL-C値を

低下させる作用を持つ薬物である．エゼチミブは，TG値が正常値の患者ではTG値に影響しないが，高TG血症患者(TG≧150 mg/dl)ではTGを17%程度低下させ，低HDL血症患者ではHDL-C値を17%程度増加させる．

Miettinenらは，CADの既往のある患者を対象とした4Sのサブ解析で，コレステロール吸収が亢進した群では主要冠動脈イベント再発リスクが有意に高く，シンバスタチン投与にても冠動脈イベントを抑制できないと報告している[14]．また，DEBATE studyでは，コレステロール吸収が低い群に比しコレステロール吸収が高い群では脳・心血管イベントの頻度が有意に高値であった[15]．これらのデータから，コレステロール吸収の促進が心血管イベントのリスクとなっていることが示唆されていた．

エゼチミブは，ABCG5あるいはABCG8の遺伝子変異によるシトステロール血症において，血中に増加する植物性ステロール(シトステロール，カンペステロールなど)を低下させ，黄色腫の消褪を来す効果が報告されている[16]．エゼチミブは，スタチンと併用することによりautosomal recessive hypercholesterolemia(ARH)症例に対してLDL-C値を著明に低下させる報告もなされている[17]．

最近発表されたENHANCE試験[18]は，家族性高コレステロール血症(FH)ヘテロ接合体に対してシンバスタチン80 mg/日，あるいはシンバスタチン80 mg/日＋エゼチミブ10 mg/日の2年間併用投与による頸動脈内膜複合体厚(IMT)の変化をみたランダム化二重盲検比較対象試験である．シンバスタチン単独投与群に比べて，シンバスタチンとエゼチミブの併用群ではLDL-C，hsCRPがさらに低下を認めたが，IMTに関しては有意な差を認めなかった．これは，薬剤開始前のIMT値が0.68～0.69 mmであり，FHとしては考えられないくらいに低値であり，積極的脂質低下療法の効果を発揮できないバックグラウンドであったことが理由として考えられる．今後の大規模臨床試験の結果が期待される．

脂質異常症の非薬物療法

FHホモ接合体は，LDL受容体遺伝子異常によって生下時より皮膚黄色腫，著明な高コレステロール血症(600～1,000 mg/dl)，若年性動脈硬化症を主徴とする疾患である[19]．コレスチラミン，HMGCoA還元酵素阻害剤などの高脂血症治療薬は，これらの主たる作用機序が肝臓におけるLDL受容体発現の増加によるものであり，FHホモ接合体にはほとんど無効である．そこで薬物療法の限界を克服する必要性からLDLを血漿中より強制的に除去する技術(LDLアフェレーシス)が開発されてきた．LDLアフェレーシス療法は，当初FHホモ接合体の治療法として開発されたが，冠動脈疾患を有し，スタチンで十分な効果を得られないFHヘテロ接合体にも適応とされ，閉塞性動脈硬化症(ASO)や巣状糸球体硬化症(FGS)に対する治療法としても確立している．

1．LDLアフェレーシス

1) LDLアフェレーシスの方法

① 単純血漿交換法(plasma exchange)

1975年，Thompsonらによって行われたFHで，高コレステロール血症の是正，冠動脈狭窄の改善を伴う狭心痛の軽減，黄色腫の消褪といった臨床症状の著明な改善を認めた最初のアフェレーシス法である[20]．単純血漿交換療法は，血漿成分を遠心分離法または膜分離法により分離除去して，ヒトアルブミン製剤を補う方法である(図1a)．単純血漿交換療法によりLDL-C値は低下し，定期的に治療を継続することで皮膚黄色腫や腱黄色腫は退縮する．この方法では除去する物質に選択性がなく，血漿成分がすべて除かれるため，免疫グロブリンの低下，HDL-C値の低下が問題になる．しかし，次に述べるより選択的なLDL除去を行う二重膜濾過法や選択的LDL吸着療法は体外循環量が大きく，体重が30 kg以下の小児には施行することができない．したがって，本法がFHに対して行われるのは，こうした小児例に限られる．

② 二重膜濾過法

二重膜濾過法は，一次膜フィルターによって分離された血漿成分を二次膜フィルターにおいて分

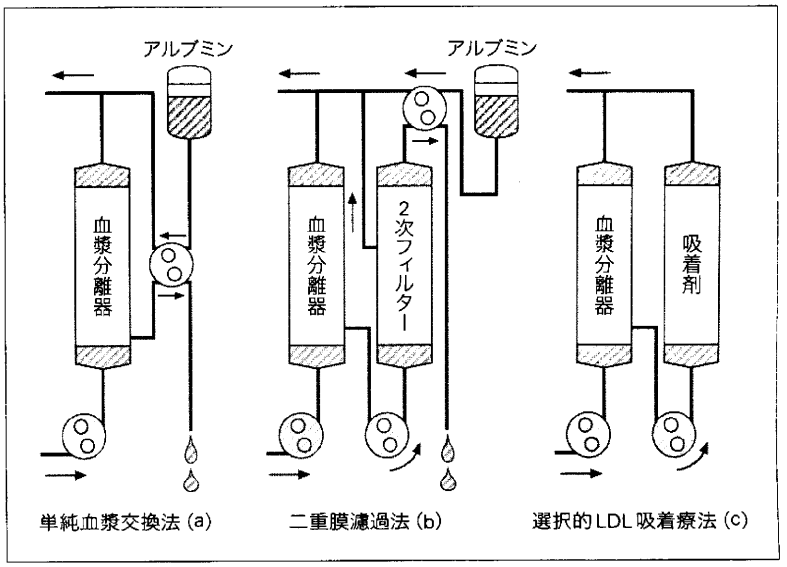

図1　LDLアフェレーシスの方法

子の大きさでふるいにかけ，巨大粒子であるVLDLおよびLDLを選択的に除去する治療法である(**図1b**)．VLDL，LDLの低下とともに，比較的大分子量を持つHDL，免疫グロブリンやフィブリノーゲンにもある程度の低下を認める．本法は，選択性においては次に述べる選択的LDL吸着療法には及ばないが，低コストであり，黄色腫の退縮だけでなく，動脈硬化性病変の退縮の報告もある．

③ 選択的LDL吸着療法

LDLがデキストラン硫酸に選択的に結合する事実をもとに日本で開発されたのが選択的LDL吸着療法である．血液を血球成分と血漿成分に分画した後，陰性に荷電したデキストラン硫酸をリガンドとして多孔質ビーズに固定したカラムを通過させ，プラスに荷電したアポリポ蛋白Bを含むリポ蛋白〔VLDL，LDL，Lp(a)〕を特異的に除去する方法である(**図1c**)[21,22]．アポBを含まない粒子は除去されず，HDL-C値の低下を認めない．

LDL除去にはカラム(LA 15)2本を用い，吸着されたLDLを高濃度NaCl(5%)によって溶出させ交互に用いる方法(LA 15システム)がとられている．この方法は小容量のLDL吸着カラムの再利用を繰り返すことで，その飽和によってLDL除去効果が失われることを防いでおり，処理血漿量が増加してもLDL除去能の低下が起こらない．したがって，体外循環量が小さく押さえられており，心負担が軽く，心機能低下や低体重の症例にも比較的安全に使用できる．ただし，LDL吸着カラムは陰性荷電を持つため，抗凝固剤にヘパリンを用いた場合，血液凝固系を活性化しブラディキニンが上昇することが知られており，アンジオテンシン変換酵素(ACE)阻害剤との併用はブラディキニン産生を急上昇させアナフィラキシー症状を引き起こすことがあるため禁忌である．

選択的LDL吸着療法は，LDLを低下するのみでなく，細胞接着因子(ICAM-1，ELAM-1など)の発現抑制，フィブリノーゲン，凝固因子の低下などによる血栓形成の抑制，血液粘度の改善，LDLの亜分画の改善，LDLの被酸化能の改善，アフェレーシス施行後のHDLの上昇，血管内皮機能の改善などを通しても抗動脈硬化作用を持つことが期待されている．

2) LDLアフェレーシスの治療開始時期

FHホモ接合体はLDL-アフェレーシスの絶対適応であり，できる限り早期にLDLアフェレー

シス治療を開始すべきである．現実的な治療開始の時期は，ベッド上で臥床し体外循環施行が可能となる4〜6歳頃からとなるが，3.5歳時に開始した例の報告もある．乳児期にすでに冠動脈狭窄や完全閉塞，大動脈弁狭窄や弁上狭窄を有する例も存在し，開始の時期が遅くなるほど予後が悪くなるので，できる限り早期に治療を開始することが勧められる．

3) FHホモ接合体に対するLDLアフェレーシスの長期治療効果

FHホモ接合体に対するLDLアフェレーシス治療の長期効果については，皮膚黄色腫の退縮，狭心症の症状の軽快，冠動脈の動脈硬化性病変の進展の抑制，退縮効果など，長期間の良好な治療効果の報告も多い．一方，FHホモ接合体に対して，LDLアフェレーシスの導入が遅れると，心筋梗塞での死亡例の報告もあり，早期のLDLアフェレーシスの導入が望まれる．

4) FHヘテロ接合体に対するLDLアフェレーシスの長期治療効果

FHヘテロ接合体については，Mabuchiらは LDLアフェレーシス施行群(43例)と薬物療法群(87例)の総死亡，心血管イベント数を比較し，平均観察期間6年間で，薬物療法群よりLDLアフェレーシス施行群のほうが心血管イベント数が低いこと，しかし，総死亡においては有意差がないことを報告している[23]．Randomized control studyとしては，ThompsonがFamilial Hypercholesterolemia Regression Studyとして報告している．39名のFHヘテロ接合体患者をシンバスタチン 40 mg/日とcolestipol 20 g/日の薬物療法群とシンバスタチン40 mg/日とLDLアフェレーシス療法(デキストラン硫酸カラム)併用群の2群に無作為に割り付け比較し，2年後に薬物療法群と比較してアフェレーシス併用群では，LDLコレステロール，Lp(a)が有意に低下していたが，冠動脈造影所見は両群に有意差はなかった[24]．LDL-Apheresis Atherosclerosis Regression Study(LAARS)[25]では，男性FH患者42名をシンバスタチン40 mg/日を用いた薬物療法群と，シンバスタチン40 mg/日にLDLアフェレーシス療法(デキストラン硫酸カラム：頻度は2週に1回)を併用した群の2群に無作為に割り付け，2年間の観察期間で死亡，心血管イベント数に有意差はないものの，LDLアフェレーシス療法併用群において冠動脈粥腫の退縮効果が大きいこと，冠血流が有意に高いことを報告している．

2．その他の治療法

FHホモ接合体に対して，門脈下大静脈吻合術，肝臓移植，遺伝子治療などが行われたことがある．

1) 門脈下大静脈吻合術

FHホモ接合体患者に対して，門脈下大静脈吻合術(portacaval shunt)が行われていたことがあり，コレステロール値の改善，黄色腫の退縮を認めている．わが国でも1例の報告があるが，侵襲が大きいわりに効果が少なく，LDLアフェレーシスにてLDL-C値の低下が可能になった現在は行われていない．

2) 肝臓移植

FHホモ接合体に対して心肝同時移植が行われたことがある．肝移植後数日にして血清コレステロール値は前値の4分の1以下になり，さらにスタチンを併用することにより血清コレステロール値は正常化した．また，わが国でも生体肝移植例の報告がある[26,27]．しかし，死亡例の報告も複数あり，侵襲が大きいうえに免疫抑制剤を長期に使用しなければならないことなど，その長期予後に対する評価は定まっていない．

3) 遺伝子治療

FHホモ接合体患者に対して*ex vivo*法を用いた遺伝子治療の臨床試験が報告されている．5例のFHホモ接合体患者に対し，肝臓の一部を切除して肝細胞を取り，培養してレトロウイルスを用いてLDL受容体遺伝子を導入し，門脈カテーテルを介してLDL受容体を発現している肝細胞を再注入する方法である．5例のうち3例に6〜25%のLDL-C値の低下を認め，4カ月後の肝生検において5例すべてにLDL受容体の発現を認めたと報告された[28]．この遺伝子治療の1例目の報告がなされた直後に，LDL受容体の発見者であるBrown，Goldsteinらは，その有効性に疑問を呈している[29]．LDL受容体の機能が低下して

いるタイプ(receptor defective type)の場合，手術の侵襲のために内因性のLDL受容体の発現が増強してLDL-C値が低下する場合があるために導入遺伝子が発現していることを検証することが重要であるという彼らのコメントが掲載された．その後，この治療は行われていない．

近年，FHホモ接合体の新しい治療法として，アポBに対するアンチセンスの投与法が開発された[30]．36人の軽度の高脂血症患者に二重盲検法によりアポBに対するアンチセンス(ISIS 301012)を皮下注射した結果，LDL-C値は35%の低下を認めている[31]．

おわりに

スタチンの発見，ストロングスタチンの開発，LDLアフェレーシスの開発など，この約20年間に脂質異常症に対する薬物療法および非薬物療法治療が確立し，冠動脈疾患をはじめとした動脈硬化症の予防が可能となった．これらの治療法の開発のうえで，日本が中心的な役割を果たしていることは特記すべきことである．

文 献

1) Dawber TR, Moore FE, Mann GV: Coronary heart disease in the Framingham study. Am J Public Health Nations Health 47(4 Pt 2): 4-24, 1957
2) 日本動脈硬化学会：動脈硬化性疾患予防ガイドライン，2007年版
3) Endo A, Kuroda M, Tsujita Y: ML-236A, ML-236B, and ML-236C, new inhibitors of cholesterogenesis produced by *Penicillium citrinium*. J Antibiot(Tokyo) 29: 1346-1348, 1976
4) Nakamura H, Arakawa K, Itakura H, et al: Primary prevention of cardiovascular disease with pravastatin in Japan(MEGA Study): a prospective randomised controlled trial. Lancet 368: 1155-1163, 2006
5) The Lipid Research Clinics Coronary Primary Prevention Trial results. I. Reduction in incidence of coronary heart disease. JAMA 251: 351-364, 1984
6) The Lipid Research Clinics Coronary Primary Prevention Trial results. II. The relationship of reduction in incidence of coronary heart disease to cholesterol lowering. JAMA 251: 365-374, 1984
7) Baxter JD, Webb P: Metabolism: bile acids heat things up. Nature 439: 402-403, 2006
8) Frick MH, Elo O, Haapa K, et al: Helsinki Heart Study: primary-prevention trial with gemfibrozil in middle-aged men with dyslipidemia. Safety of treatment, changes in risk factors, and incidence of coronary heart disease. N Engl J Med 317: 1237-1245, 1987
9) Lipids and lipoproteins in symptomatic coronary heart disease. Distribution, intercorrelations, and significance for risk classification in 6,700 men and 1,500 women. The Bezafibrate Infarction Prevention(BIP) Study Group, Israel. Circulation 86: 839-848, 1992
10) Keech A, Simes RJ, Barter P, et al: Effects of long-term fenofibrate therapy on cardiovascular events in 9,795 people with type 2 diabetes mellitus(the FIELD study): randomised controlled trial. Lancet 366: 1849-1861, 2005
11) Kita T, Nagano Y, Yokode M, et al: Probucol prevents the progression of atherosclerosis in Watanabe heritable hyperlipidemic rabbit, an animal model for familial hypercholesterolemia. Proc Natl Acad Sci USA 84: 5928-5931, 1987
12) Tardif JC, Cote G, Lesperance J, et al: Probucol and multivitamins in the prevention of restenosis after coronary angioplasty. Multivitamins and Probucol Study Group. N Engl J Med 337: 365-372, 1997
13) Yokoi H, Daida H, Kuwabara Y, et al: Effectiveness of an antioxidant in preventing restenosis after percutaneous transluminal coronary angioplasty: the Probucol Angioplasty Restenosis Trial. J Am Coll Cardiol 30: 855-862, 1997
14) Miettinen TA, Gylling H, Strandberg T, Sarna S: Baseline serum cholestanol as predictor of recurrent coronary events in subgroup of Scandinavian simvastatin survival study. Finnish 4S Investigators. BMJ 316: 1127-1130, 1998
15) Strandberg TE, Tilvis RS, Pitkala KH, et al: Cholesterol and glucose metabolism and recurrent cardiovascular events among the elderly: a prospective study. J Am Coll Cardiol 48: 708-714, 2006
16) Darkes MJ, Poole RM, Goa KL: Ezetimibe. Am J Cardiovasc Drugs 3: 67-76, discussion 77-68, 2003
17) Lind S, Olsson AG, Eriksson M, et al: Autosomal recessive hypercholesterolaemia: normalization of plasma LDL cholesterol by ezetimibe in combination with statin treatment. J Intern Med 256: 406-412, 2004
18) Kastelein JJ, Akdim F, Stroes ES, et al: Simvastatin with or without ezetimibe in familial hypercholesterolemia. N Engl J Med 358: 1431-1443, 2008
19) Goldstein JL, Hobbs HH, Brown MS: Familial hypercholesterolemia. In: Scriver CR, et al(eds), The Metabolic and Molecular Basis of Inherited Disease, 8 edn, vol. 2. McGraw-Hill, New York, pp2863-2913, 2001

20) Thompson GR, Lowenthal R, Myant NB: Plasma exchange in the management of homozygous familial hypercholesterolaemia. Lancet 1: 1208-1211, 1975
21) Yokoyama S, Hayashi R, Kikkawa T, et al: Specific sorbent of apolipoprotein B-containing lipoproteins for plasmapheresis. Characterization and experimental use in hypercholesterolemic rabbits. Arteriosclerosis 4: 276-282, 1984
22) Yokoyama S, Hayashi R, Satani M, et al: Selective removal of low density lipoprotein by plasmapheresis in familial hypercholesterolemia. Arteriosclerosis 5: 613-622, 1985
23) Mabuchi H, Koizumi J, Shimizu M, et al: Long-term efficacy of low-density lipoprotein apheresis on coronary heart disease in familial hypercholesterolemia. Hokuriku-FH-LDL-Apheresis Study Group. Am J Cardiol 82: 1489-1495, 1998
24) Thompson GR, Maher VM, Matthews S, et al: Familial Hypercholesterolaemia Regression Study: a randomised trial of low-density-lipoprotein apheresis. Lancet 345: 811-816, 1995
25) Tatami R, Inoue N, Itoh H, et al: Regression of coronary atherosclerosis by combined LDL-apheresis and lipid-lowering drug therapy in patients with familial hypercholesterolemia: a multicenter study. The LARS Investigators. Atherosclerosis 95: 1-13, 1992
26) Kawagishi N, Satoh K, Akamatsu Y, et al: Long-term outcome after living donor liver transplantation for two cases of homozygous familial hypercholesterolemia from a heterozygous donor. J Atheroscler Thromb 14: 94-98, 2007
27) Shirahata Y, Ohkohchi N, Kawagishi N, et al: Living-donor liver transplantation for homozygous familial hypercholesterolemia from a donor with heterozygous hypercholesterolemia. Transpl Int 16: 276-279, 2003
28) Grossman M, Raper SE, Kozarsky K, et al: Successful *ex vivo* gene therapy directed to liver in a patient with familial hypercholesterolaemia. Nat Genet 6: 335-341, 1994
29) Brown MS, Goldstein JL, Havel RJ, et al: Gene therapy for cholesterol. Nat Genet 7: 349-350, 1994
30) Crooke RM, Graham MJ, Lemonidis KM, et al: An apolipoprotein B antisense oligonucleotide lowers LDL cholesterol in hyperlipidemic mice without causing hepatic steatosis. J Lipid Res 46: 872-884, 2005
31) Kastelein JJ, Wedel MK, Baker BF, et al: Potent reduction of apolipoprotein B and low-density lipoprotein cholesterol by short-term administration of an antisense inhibitor of apolipoprotein B. Circulation 114: 1729-1735, 2006

Intratracheal Gene Transfer of Adrenomedullin Using Polyplex Nanomicelles Attenuates Monocrotaline-induced Pulmonary Hypertension in Rats

Mariko Harada-Shiba[1], Itaru Takamisawa[1], Kanjiro Miyata[2,3], Takehiko Ishii[2,3], Nobuhiro Nishiyama[3,4], Keiji Itaka[3,4], Kenji Kangawa[5], Fumiki Yoshihara[6], Yujiro Asada[7], Kinta Hatakeyama[7], Noriya Nagaya[8] and Kazunori Kataoka[3,4,9]

[1]Department of Bioscience, National Cardiovascular Center Research Institute, Suita, Japan; [2]Department of Bioengineering, Graduate School of Engineering, The University of Tokyo, Tokyo, Japan; [3]Center for NanoBio Integration, The University of Tokyo, Tokyo, Japan; [4]Division of Clinical Biotechnology; Center for Disease Biology and Integrative Medicine, Graduate School of Medicine, The University of Tokyo, Tokyo, Japan; [5]National Cardiovascular Center Research Institute, Suita, Japan; [6]Division of Hypertension and Nephrology, National Cardiovascular Center, Suita, Japan; [7]Department of Pathology, Faculty of Medicine, University of Miyazaki, Miyazaki, Japan; [8]Department of Regenerative Medicine, National Cardiovascular Center Research Institute, Suita, Japan; [9]Department of Materials Engineering, Graduate School of Engineering, The University of Tokyo, Tokyo, Japan

Pulmonary arterial hypertension (PAH) is a life-threatening disease characterized by progressive PAH and right ventricular failure. Despite recent advances in therapeutic approaches using prostanoids, endothelin antagonists, and so on, PAH remains a challenging condition. To develop a novel therapeutic approach, we have established a nonviral gene delivery system of poly(ethylene glycol) (PEG)-based block catiomers, which form a polyplex nanomicelle with a nanoscaled core–shell structure in the presence of DNA. The polyplex nanomicelle from PEG-*b*-poly{*N*-[*N*-(2-aminoethyl)-2-aminoethyl]aspartamide} (PEG-*b*-P[Asp(DET)]), having ethylenediamine units at the side chain, showed ~100-fold increase in luciferase transgene expression activity in mouse lung via intratracheal administration with a minimal toxicity compared with the polyplex from linear poly(ethylenimine) (LPEI). The transfection activity was highest on day 3 after administration and remained detectable until day 14. PEG-*b*-P[Asp(DET)] polyplex nanomicelles were formulated with a therapeutic plasmid bearing the human adrenomedullin (*AM*) gene and intratracheally administered to rats with monocrotaline-induced pulmonary hypertension. The right ventricular pressure significantly decreased 3 days after administration as confirmed by a notable increase of pulmonary human AM mRNA levels. Intratracheal administration of PEG-*b*-P[Asp-(DET)] polyplex nanomicelles showed remarkable therapeutic efficacy with PAH animal models without compromising biocompatibility.

Received 29 July 2008; accepted 9 March 2009; published online 31 March 2009. doi:10.1038/mt.2009.63

INTRODUCTION

Idiopathic pulmonary arterial hypertension (PAH) is a rare disease characterized by a progressive increase in pulmonary vascular resistance, leading to right heart failure and death.[1] Recent advances in therapeutic approaches to PAH show promising targeting pathways believed to play critical pathogenic or pathophysiologic roles;[2] however, despite these findings, PAH remains a challenging condition.[3]

Adrenomedullin (AM), a peptide isolated from human pheochromocytoma,[4] has multiple beneficial effects on cardiovascular tissues, including a powerful hypotensive effect.[5] Moreover, AM is indicated for PAH because of its prodilatory effects and the abundance of AM receptors in the lung.[6] Inhalation of AM was reported to ameliorate PAH in animal models[7] as well as in PAH patients without inducing systemic hypotension, but this effect was transient.[8] To overcome these barriers, a new, efficacious, and long-lasting AM therapy for PAH is warranted.

Gene therapy is one of the strategic approaches to continuously supply therapeutic peptides or proteins to target tissues.[6] Gene delivery to the lung via inhalation can avoid many problems associated with intravenous delivery, such as immediate nuclease degradation in the blood stream and the difficulty associated with penetrating endothelial barriers. In this regard, AM-based gene therapy through intratracheal route for PAH may have a promise.[7] Successful gene delivery via inhalation strongly depends on the development of advanced gene vectors to protect the therapeutic plasmid, provide site-specific targeting, and effectively release these plasmids for the desired pharmacological effect.

To develop a novel gene therapy system, we utilized our established polymeric library consisting of poly(ethylene glycol) (PEG)-based block catiomers, which form core–shell polyplex nanomicelles with core sequestration of the therapeutic plasmid.[9,10]

Correspondence: *Mariko Harada-Shiba, Department of Bioscience, National Cardiovascular Center Research Institute, 5-7-1 Fujishirodai, Suita, Osaka 565-8565, Japan. E-mail: mshiba@ri.ncvc.go.jp*

These polyplex nanomicelles are well dispersed even in aqueous media containing serum proteins and protect plasmid DNA from degradation by nuclease *in vivo*.[11–13] We recently developed P[Asp(DET)], a poly(aspartamide) derivative bearing an *N*-(2-aminoethyl)aminoethyl group as the side chain, that showed improved transfection efficiency and biocompatibility compared to linear poly(ethylenimine) (LPEI).[14] The PEG-based block catiomer with P[Asp(DET)] was applied *in vivo* to deliver therapeutic plasmids for a murine, skull bone defect model and a rabbit carotid artery with neointima model; its successful therapeutic efficacy with these mammalian studies provided the impetus for expanded application into the treatment of intractable diseases suited for gene therapy.[15,16]

In this paper, we report advanced, pulmonary transfection efficiencies using intratracheally inhaled PEG-*b*-P[Asp(DET)] polymeric nanomicelles without compromising biocompatibility. The intratracheal administration of the *AM* gene by PEG-*b*-P[Asp-(DET)] polyplex nanomicelles reduced right ventricular pressure in PAH animal models without inducing inflammation, suggesting its suitability as a vector for translational research.

RESULTS

Reporter gene transfer using PEG-*b*-P[Asp(DET)] via intratracheal administration

Plasmids bearing the luciferase reporter gene were formulated with PEG-*b*-P[Asp(DET)] (N/P = 80) and LPEI (N/P = 6) and were sprayed intratracheally into ICR mice. Here, N/P ratio refers to the unit molar ratio of the amino group in the polymer to the phosphate group in the plasmid DNA. After 1 day, the mice were killed and the pulmonary tissues were harvested to quantify luciferase activity. PEG-*b*-P[Asp(DET)] polyplex nanomicelles showed nearly a 100-fold increase in luciferase levels than the LPEI controls (**Figure 1**). **Figure 2** shows the time-dependent changes of luciferase gene expression in the pulmonary tissue with PEG-*b*-P[Asp(DET)] polyplex nanomicelles. Luciferase activity was highest on day 3, and remained detectable until day 14. To elucidate the effect of PEG-*b*-P([Asp(DET)]/pLuc N/P ratios on luciferase gene expression, a series of the nanomicelles formulated under the varying N/P ratios (20, 40, and 80) were also examined. **Figure 3** shows an ~50-fold increase in luciferase expression from N/P = 20 to N/P = 80 over a 3-day period. Next, PEG-*b*-P[Asp(DET)] polyplex nanomicelles loaded with plasmid DNA bearing the yellow fluorescence protein (YFP) gene (N/P = 80) or LPEI/pYFP polyplexes (N/P = 6) were sprayed intratracheally in ICR mice. After 1 day, the pulmonary tissue was harvested and the YFP gene expression was visualized by fluorescence microscopy (**Figure 4**). Significantly higher fluorescence intensity was clearly seen in the lungs treated with the PEG-*b*-P[Asp(DET)] polyplex nanomicelle than the LPEI polyplexes; moreover, YFP fluorescence activity was distinctly visible for the animals treated with PEG-*b*-P[Asp(DET)] polyplex micelles in the secondary bronchi and lower pulmonary generations. To evaluate the toxicity, immunohistochemistry was conducted on the lung tissues after the transfection of LPEI/pLuc controls (N/P = 6) (**Figure 5a–c**) or PEG-*b*-P[Asp(DET)]/pLuc (N/P = 80) (**Figure 5d–f**). The lung administered with LPEI/pLuc showed moderate infiltration of neutrophils at the

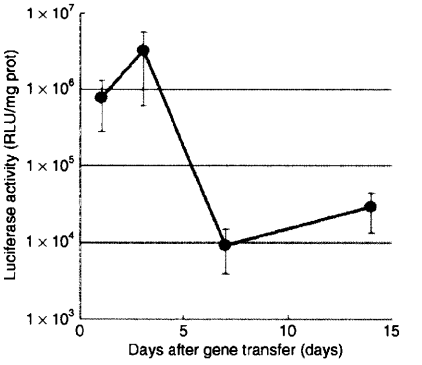

Figure 2 Time-dependent changes in gene expression after intratracheal administration of PEG-*b*-P[Asp(DET)] polyplex nanomicelle loaded with luciferase gene. The mice (five mice per group) were anesthetized and the polyplex nanomicelle was administered intratracheally. After the indicated time, the lung tissues were harvested, homogenized, and measured for luciferase activity (mean ± SEM, *N* = 5). PEG-*b*-P[Asp(DET)], PEG-*b*-poly{*N*-[*N*-(2-aminoethyl)-2-aminoethyl]aspartamide}.

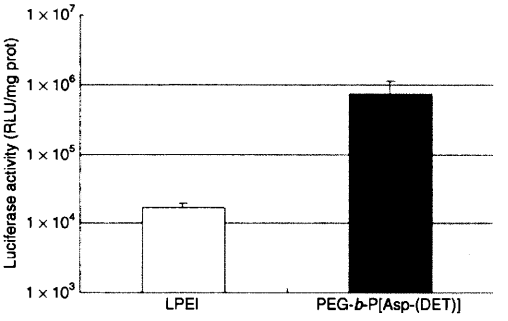

Figure 1 Luciferase gene expression by intratracheal administration of LPEI polyplex (N/P = 6) or PEG-*b*-P[Asp(DET)] polyplex nanomicelle (N/P = 80). Samples of the polyplex and the polyplex nanomicelle were prepared before the administration and left for 1 day. The mice (five mice per group) were anesthetized and the polyplex or the polyplex nanomicelle was administered intratracheally. At 24 hour postadministration, the lung tissues were harvested, homogenized, and measured for luciferase activity (mean ± SEM, *N* = 5). LPEI, linear poly(ethylenimine); PEG-*b*-P[Asp(DET)], PEG-*b*-poly{*N*-[*N*-(2-aminoethyl)-2-aminoethyl]aspartamide}.

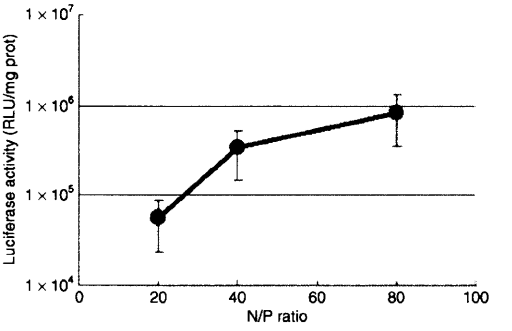

Figure 3 Charge-ratio-dependent changes in gene expression after intratracheal administration of the PEG-*b*-P[Asp(DET)] polyplex nanomicelle loaded with luciferase gene. The mice (five mice per group) were anesthetized and the polyplex nanomicelle was administered intratracheally. At 3 days postadministration, the lung tissues were harvested, homogenized, and measured for luciferase activity (mean ± SEM, *N* = 5). PEG-*b*-P[Asp(DET)], PEG-*b*-poly{*N*-[*N*-(2-aminoethyl)-2-aminoethyl]aspartamide}.

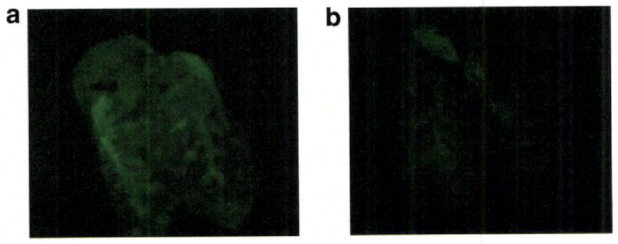

Figure 4 Fluorescence photographs of lungs transfected by intratracheal administration of YFP gene using PEG-*b*-P[Asp(DET)] polyplex nanomicelle or LPEI polyplex. (**a**) PEG-*b*-P[Asp(DET)] polyplex nanomicelle (N/P = 80), (**b**) LPEI polyplex (N/P = 6). The lung specimens were observed under a fluorescence microscope (SZX12; Olympus). LPEI, linear poly(ethylenimine); PEG-*b*-P[Asp(DET)], PEG-*b*-poly{*N*-[*N*-(2-aminoethyl)-2-aminoethyl]aspartamide}.

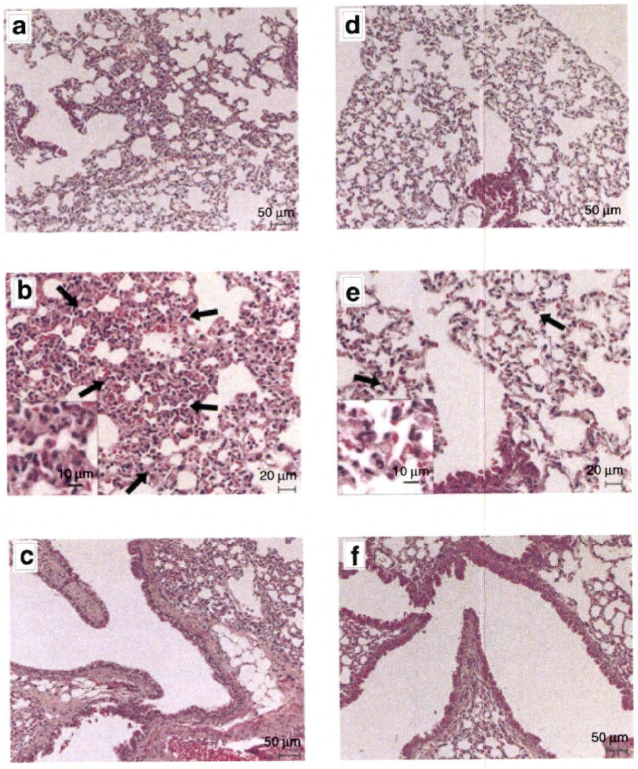

Figure 5 Representative photomicrographs of lung tissues 7 days postintratracheal administration of LPEI/pLuc (N/P = 6) (**a–c**) or PEG-*b*-P[Asp(DET)]/pLuc (N/P = 80) (**d–f**). The terminal bronchiole and alveoli of the lungs administered with LPEI polyplex (**a**,**b**) and PEG-*b*-P[Asp(DET)] polyplex nanomicelle (**d**,**e**) are shown. The neutrophil infiltration is indicated with arrows in the photomicrographs with higher magnification (**b**,**e**). Each inset is the picture with higher magnification. The bronchus of the lungs administered with LPEI polyplex (**c**) and PEG-*b*-P[Asp(DET)] polyplex nanomicelle (**f**) are also shown. LPEI, linear poly(ethylenimine); PEG-*b*-P[Asp(DET)], PEG-*b*-poly{*N*-[*N*-(2-aminoethyl)-2-aminoethyl]aspartamide}.

terminal bronchiole and alveoli as indicated (Figure 5a,b). However, the lung administered with PEG-*b*-P[Asp(DET)]/pLuc, neutrophilic infiltration was scattered and minimal or absent (Figure 5d,e). No apparent inflammatory infiltrate was observed in the bronchus of the both groups (Figure 5c,f). The findings thereby supported increased biocompatibility with the PEG-*b*-P[Asp(DET)] polyplex micelle. To further evaluate the toxicity of the gene carrier systems, mRNA levels of inflammatory cytokines in the pulmonary tissue were measured using real-time reverse transcriptase (RT)-PCR. A nontreated cohort was used as a control. Proinflammatory cytokine mRNA levels did not increase for intratracheally administered naked pLuc in saline or the PEG-*b*-P[Asp(DET)] polyplex micelles; however, LPEI/pLuc polyplexes revealed a twofold increase in TNF-α, interleukin (IL)-6, IL-10, and Cox-2 compared to the control (Figure 6a–d). Notably, PEG-*b*-P[Asp(DET)]/pLuc proinflammatory levels were statistically similar to the negative control cohorts in TNF-α, IL-6, IL-10, and Cox-2 mRNA levels.

Effect of *AM* gene transfer by PEG-*b*-P[Asp(DET)] polyplex nanomicelle in a rat model of PAH

After 4 weeks of monocrotaline injection, right ventricular pressure was increased to twice of the normal value (Figure 7). Notably, right ventricular pressure was decreased significantly by an intratracheal spray of the PEG-*b*-P[Asp(DET)] polyplex nanomicelle loaded with the expression vector of AM (N/P = 40). On the other hand, right ventricular pressure did not change significantly after administration of naked plasmid encoding the *AM* gene in saline or the LPEI polyplex loaded with the *AM* gene, or the polyplex nanomicelle loaded with the luciferase gene. The mRNA levels of human AM in the lung were measured by real-time RT-PCR (Figure 8). The lung transfected with the polyplex nanomicelle loaded with the expression vector of AM had high levels of AM mRNA. Alternatively, the levels were much lower in the lung transfected with the LPEI polyplex loaded with the expression vector of AM. The lung transfected with the polyplex nanomicelle loaded with the luciferase gene or with the naked *AM* gene in saline showed no expression of human AM.

DISCUSSION

The large number of human diseases presenting poor prognoses and limited efficacy with current therapeutic regimens necessitates the advent of alternative approaches. PAH is such a disease without a highly efficacious therapeutic regimen.[17] PAH patients are currently treated with a variety of drugs including prostacyclin, prostacyclin analogues, calcium channel blockers, nitric-oxide inhalation, angiotensin-converting enzyme inhibitors, endothelin receptor antagonists, and phosphodiesterase type 5 inhibitors; in severe cases lung transplantation and subsequent immunosuppression are necessary.[17] However, promising alternative therapies for PAH have been recently reported. For example, Champion *et al.* reported that adenoviral gene transfer of endothelial nitric-oxide synthase to the lungs of endothelial nitric-oxide synthase knockout mice ameliorates the symptoms of PAH.[18] Champion *et al.* also reported that adenoviral gene transfer of calcium gene-related peptide attenuates the symptoms of PAH.[19] Nagaya *et al.* reported that transfection of human prostacyclin synthase using hemagglutinating virus of Japan–liposomes ameliorates monocrotaline-induced PAH.[20] However, in these attempts, viral or viral-related vectors were used for the delivery of therapeutic genes and these gene carriers have the potential for immunogenicity and inflammatory response. In diseases where a single dose can cure or provide palliative care, viral vectors may be suitable; however, PAH therapy requires repeated

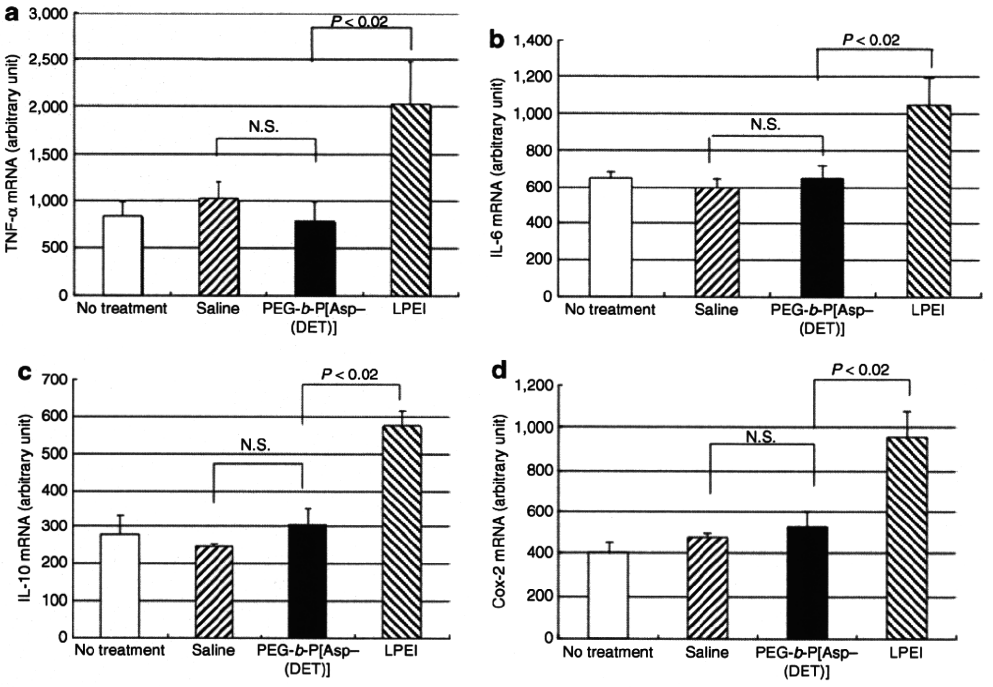

Figure 6 mRNA expression of inflammatory cytokines in lung tissues 7 days postintratracheal administration of luciferase gene in saline; LPEI polyplex with luciferase gene (N/P = 6); or PEG-*b*-P[Asp(DET)] polyplex nanomicelle with luciferase gene (N/P = 80) (mean ± SEM, $N = 4$). (**a**) TNF-α, (**b**) IL-6, (**c**) IL-10, (**d**) Cox-2. IL, interleukin; LPEI, linear poly(ethylenimine); TNF, tumor necrosis factor; PEG-*b*-P[Asp(DET)], PEG-*b*-poly{*N*-[*N*-(2-aminoethyl)-2-aminoethyl]aspartamide}.

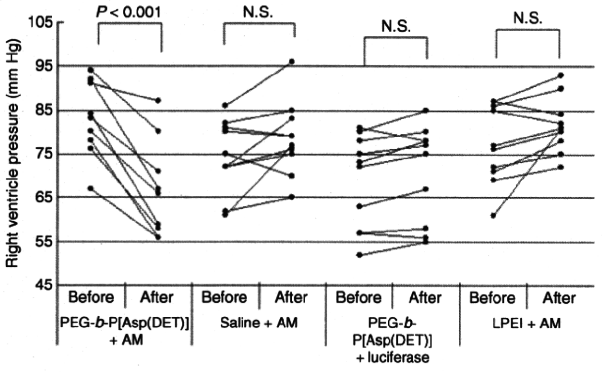

Figure 7 Effect of gene transfer on the right ventricle pressure in the PAH rat model. At 4 weeks after subcutaneous monocrotaline injection, a hemodynamic study was performed to measure the RV pressure indicated as "Before". The PEG-*b*-P[Asp(DET)] polyplex nanomicelle loaded with AM expression vector; AM expression vector in saline; PEG-*b*-P[Asp(DET)] polyplex micelle loaded with luciferase gene; or the LPEI polyplex loaded with AM expression vector were sprayed intratracheally. Three days later, a hemodynamic study was performed again to measure the RV pressure indicated as "After". AM, adrenomedullin; LPEI, linear poly(ethylenimine); PAH, pulmonary arterial hypertension; PEG-*b*-P[Asp(DET)], PEG-*b*-poly{*N*-[*N*-(2-aminoethyl)-2-aminoethyl]aspartamide}; RV, right ventricular.

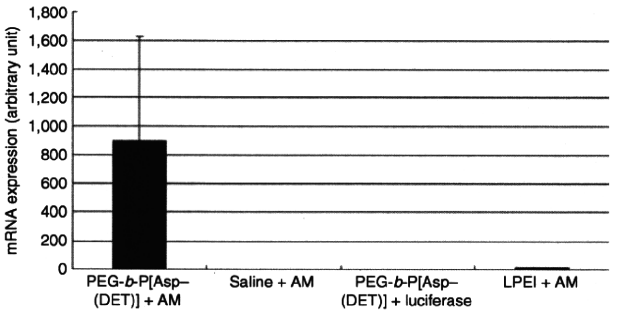

Figure 8 mRNA expression of human AM in the PAH rat model postintratracheal administration of PEG-*b*-P[Asp(DET)] polyplex nanomicelles loaded with the AM expression vector; AM expression vector in saline; PEG-*b*-P[Asp(DET)] polyplex nanomicelles loaded with the luciferase gene; or LPEI polyplexes loaded with the AM expression vector. Rats were transfected intratracheally at 4 weeks after subcutaneous monocrotaline injection. Three days later, lungs were harvested, homogenized, and measured for AM mRNA using real-time RT-PCR (mean ± SEM, $N = 4$). AM, adrenomedullin; LPEI, linear poly(ethylenimine); PAH, pulmonary arterial hypertension; PEG-*b*-P[Asp(DET)], PEG-*b*-poly{*N*-[*N*-(2-aminoethyl)-2-aminoethyl]aspartamide}.

administrations for efficacy, hence the utility of viral or viral-based gene therapy is contraindicated.

Alternatively, nonviral gene carriers have been recognized with several advantages over viral vectors in terms of safety, immunogenicity, and ease of manufacture. To develop a method of gene therapy suitable for clinical translation, four primary factors must be clearly addressed: (i) the gene carrier, (ii) the therapeutic gene, (iii) the route of administration, and (iv) patient compliance. In this study, we chose to further explore the promising (i) PEG-*b*-P[Asp(DET)] polyplex nanomicelle nonviral gene carrier system based upon our previous findings. Next, we chose (ii) *AM* as the therapeutic gene because of its reported effectiveness in the transient treatment of PAH. For the route of administration, we selected (iii) intratracheal administration to avoid the rapid propensity of nuclease degradation in the blood compartment and also that we might exploit the lung, based upon its enormous surface area, for

use as a therapeutic bioreactor for AM production. Pulmonary administration is a promising therapeutic route of administration in the clinic for its (iv) high patient compliance with utilization of an inhaler or nebulizer.

Recently, we have demonstrated that PEG-*b*-P[Asp(DET)] polyplex nanomicelles achieved amplified *in vitro* and *in vivo* transfection activity with minimal cytotoxicity.[14–16,21] With regard to the transfection mechanism, P[Asp(DET)] possesses the ethylenediamine side chain, which undergoes two-step protonation from the mono-protonated gauche form at physiological pH to di-protonated anti form at acidic pH, thereby exhibiting an effective buffering function in the acidic endosomal compartment.[22] Also, we revealed the membrane destabilization effect of P[Asp(DET)] responding to acidic endosomal pH conditions by hemolysis, leakage of cytoplasmic enzyme (lactate dehydrogenase assay), and confocal laser scanning microscopic observation.[22] Consequently, we observed the facilitated transport of Cy5-labeled plasmid DNA by the P[Asp(DET)] polyplexes from endo/lysosomal compartment into cytoplasm directly under the confocal laser scanning microscope in single cellular level.[22] Therefore, the increased transgene expression in **Figure 3** may be a result of the facilitated translocation of the polyplex nanomicelles from the endosome to the cytoplasm based on the buffering capacity (proton sponge effect) and/or endosomal membrane–destabilizing effect of P[Asp(DET)] segment. The reason why a relatively high N/P ratio was required for the efficient transfection (**Figure 3**) may be because the membrane-destabilizing effect of P[Asp(DET)] is dependent on the polymer concentration as previously reported. Nevertheless, the PEG-*b*-P[Asp(DET)] polyplex nanomicelles displayed minimal cytotoxicity even at a high N/P ratio, which may be due to the pH-sensitive properties of P[Asp(DET)] segment.[22] The highly transfectable but less cytotoxic properties of PEG-*b*-P[Asp(DET)] polyplex nanomicelles motivated us to apply them to the gene therapy of PAH animal models through the intratracheal administration in this study.

A number of nonviral vectors including polyplex and lipoplex have been applied for *in vivo* intratracheal transfection. Special notice for the pulmonary gene delivery via airways is that the lung has the features critically influencing the transfection efficiency, such as the presence of surfactant, alveolar macrophages, and mucocilliary clearance mechanisms. In the early 1990s, lipoplex was used by aerosol delivery or intratracheal instillation. However, cationic lipids were shown to have a decreased transfection efficiency due to the interaction with lung surfactant compared to cationic polymer like PEI.[23,24] To overcome the surfactant barriers, cationic emulsion was used and showed much higher transfection activity compared with lipoplexes, such as lipofectin, lipofectamine, and DMRIE/c.[25] However, even for the cationic emulsion, the luciferase activity was limited to 55 pg/mg protein, which is significantly lower than the value attained by the polyplex nanomicelles loaded with PEG-*b*-P[Asp(DET)] [3,000,000 relative light unit/mg protein (135 ng/mg protein)] as reported here. Polyplexes made from cationic polymer was reported to show higher transfection efficiency compared with cationic lipoplexes for pulmonary gene delivery via airways.[23,24] PEI or modified PEI has been shown to be one of the most effective agents for constructing gene delivery systems available today with high levels of pulmonary gene transfer by airways.[26,27] Intratracheal injection of polyplex loaded with 22 kd of LPEI (ExGen 500) showed up to 20,000–40,000 relative light unit/mg protein of luciferase activity in the lung by adjusting N/P ratio. Worth noting is that the nanomicelles achieved two orders of magnitude higher value in luciferase gene expression compared to the LPEI polyplex. Furthermore, no induction of cytokine responses is appealing for the nanomicelles over LPEI polyplex (**Figure 6**), which was reported to induce the activation of $CD8^+$ and $CD4^+$ T cells, and Fas ligand–mediated antigen-induced cell death.[28,29]

To ameliorate the symptoms of PAH in animal models, several genes have been identified including: endothelial nitric-oxide synthase, inducible nitric-oxide synthase, prostacyclin synthase, calcium gene-related peptide, vascular endothelial growth factor, and hepatocyte growth factor.[18–20,30–36] We used AM as a therapeutic gene because of its high potency and long-term effectiveness as a vasodilator in the pulmonary vascular bed.[37] The effect of pulmonary vasodilation is mediated by cyclic adenosine monophosphate–dependent and nitric oxide–dependent mechanisms.[38] PAH patients have elevated plasma AM concentrations, which increase in step with the disease's severity[39,40] often resulting in pulmonary hypotension. In previous studies, intravenous administration[41] and inhalation[8] of the AM peptide showed acute hemodynamic and hormonal efficacy in PAH patients. However, despite alternative routes of delivery, the small AM peptide was rapidly degraded *in vivo* displaying a poor pharmacokinetic profile with a temporal window of only 30–45 minutes. For the treatment of PAH, sustained effect of AM is required. In this report, the therapeutic indicator for successful nonviral AM delivery was a decrease in the right ventricular pressure. Indeed, for the polyplex nanomicelle/pAM formulation, the right ventricular pressure did decrease, but more importantly the persistence of *AM* gene expression continued within a therapeutic range for a minimum of 3 days. The results indicate that the therapeutic approach using the polyplex nanomicelle as a vector does not require chronic infusion or very frequent inhalation, which will make the therapy more clinically applicable.

In this study, we succeeded in delivering DNA to the lung via intratracheal administration using the polyplex nanomicelles, resulting in extremely improved transfection efficiency with concomitant high biocompatibility. More specifically, the lung transfected with the polyplex nanomicelle had much lower toxicity than that transfected with the LPEI polyplex, according to the histological findings and measurement of the mRNA levels of inflammatory cytokines (**Figure 6a–d**). We also developed an effective treatment for the PAH rat model by delivering the therapeutic *AM* gene with polyplex nanomicelles from PEG-*b*-P[Asp(DET)]. These results showed a significant increase in transfection efficiently *in vivo* with intratracheal administration. The PEG-*b*-P[Asp(DET)] polyplex nanomicelle delivery system clearly showed promising *in vivo* results of transgene and therapeutic AM expression, when coupled with the clear visual, localization of the polyplex nanomicelles in the pulmonary tissue and the lack of proinflammatory responses. We posit that the PEG-*b*-P[Asp(DET)] nonviral gene carrier clearly shows those characteristics requisite for novel and advanced therapeutic systems ideally suited for translational research.

MATERIALS AND METHODS

Materials. An expression vector for YFP (RIKEN, Tokyo, Japan) was amplified in competent HB101 *Escherichia coli* and purified by Plasmid Giga Kits (Qiagen, Hilden, Germany). An expression vector for luciferase with a CAG promoter was provided by RIKEN. An expression vector for human AM was constructed as follows. The *EcoRI*/*XhoI* fragment of the full-length human AM complementary DNA (cDNA)[42] was ligated into the *EcoRI*/*XhoI* site of pcDNA1 (Invitrogen, Carlsbad, CA). The restriction maps of expression vector for luciferase and human AM cDNA are listed in **Supplementary Figure S1a,b**, respectively. To confirm that pcDNA/AM encodes AM, pcDNA/AM was transfected into Chinese hamster ovary cells, and the medium and the cells were collected for the measurement of immunoreactive AM using an AM radioimmunoassay Shionogi (Cosmic, Tokyo, Japan).

Animals. Male ICR mice weighing 25–30 g were administered the reporter gene intratracheally. Male Wistar rats weighing 100–120 g were used to make a model of PAH. All protocols were performed in accordance with the guidelines of the Animal Care Ethics Committee of the National Cardiovascular Center Research Institute (Osaka, Japan).

Synthesis and characterization of PEG-b-P[Asp(DET)]. PEG-*b*-P[Asp(DET)] was prepared as previously described.[14] Briefly, PEG-poly(β-benzyl-L-aspartate) (PEG-PBLA) diblock copolymer was synthesized by the ring-opening polymerization of β-benzyl-L-aspartate *N*-carboxy-anhydride from the terminal primary amino group of α-methoxy-ω-amino PEG (M_w: 12,000; Nippon Oil and Fats, Tokyo, Japan). Gel-permeation chromatography confirmed that the copolymer was unimodal with a narrow molecular weight distribution (M_w/M_n: 1.23), and the number of benzyl-L-aspartate repeating units was calculated to be 68 by ^{1}H-NMR. The N-terminal amino group of PEG-PBLA was then acetylated using acetic anhydride in dichloromethane solution to obtain PEG-PBLA-Ac. The obtained polymer was dissolved in distilled *N,N*-dimethylformamide (Wako Pure Chemical Industries, Osaka, Japan) and reacted with diethylenetriamine (Tokyo Kasei Kogyo, Tokyo, Japan) for 24 hours at 40 °C in a dry argon atmosphere to undergo aminolysis of the benzyl side chain. After 24 hours, the solution was slowly dripped into a 10% acetic acid solution and dialyzed (Spectra/Por Membrane, 3,500 molecular weight cutoff; Spectrum Laboratories, Rancho Dominguez, CA) against 0.01 N HCl and subsequently against distilled water. The final solution was lyophilized to obtain PEG-*b*-P[Asp(DET)] as the hydrochloride salt form. ^{1}H-NMR confirmed the complete substitution of benzyl ester of the polymer with diethylenetriamine through the aminolysis reaction, as well as the chemical structure of the obtained PEG-*b*-P[Asp(DET)] block copolymer.

Preparation of polyplex nanomicelles. The PEG-*b*-P[Asp(DET)] block copolymer and plasmid DNA were separately dissolved in 10 mmol/l HEPES buffer (pH 7.4). Both solutions were mixed at the indicated nitrogen/phosphate ratios [=(total amines in cationic segment)/(phosphates in plasmid DNA)] and incubated overnight at room temperature to make PEG-*b*-P[Asp-(DET)] polyplex nanomicelle. LPEI (ExGen; Cosmo Bio, Tokyo, Japan) polyplexes were prepared by mixing plasmid DNA and LPEI according to the manufacturer's protocol.

In vivo *gene delivery by intratracheal administration.* ICR mice were anesthetized by intraperitoneal administration of pentobarbital (30 mg/kg) (Dainippon Sumitomo Pharma, Osaka, Japan). Tracheostomies were performed under sterile conditions for PEG-*b*-P[Asp-(DET)] polyplex nanomicelle or LPEI polyplex (10 μg of DNA for each mouse) in a 50 μl of solution administration by a microsprayer Model IA-1C (Penn Century, Philadelphia, PA). After the indicated time, the mice were killed by cervical dislocation and the pulmonary tissues harvested. To measure luciferase activity, the pulmonary tissues were homogenized in a lysis buffer using a polytron. The lysate was then centrifuged at 14,000*g* for 10 minutes at 4 °C, and 20 μl of the supernatant was analyzed for luciferase activity by a Luminous CT-9000D luminometer (Dia-Iatron, Tokyo, Japan), according to a previously described method.[43] Background of luciferase activity in the lung was measured from the lung of mice after administration of saline, which was <3% of the total activity of day 14. All the data of luciferase activity were obtained by subtraction of background data. To detect YFP expression, mice were killed by cervical dislocation and the lungs harvested. Frozen sections (5-μm thick) of the lung specimens were visualized by a fluorescence microscope (SZX12; Olympus, Tokyo, Japan). To examine the histological features of the lung tissue, the specimens were also fixed in 4% paraformaldehyde and embedded in paraffin. Sections (3-μm thick) were stained with hematoxylin.

Isolation of RNA and cDNA synthesis. Total RNA was extracted using the Trizol method (Gibco BRL Life Technologies, Breda, Netherlands) according to the protocol provided by the manufacturer. The RNA was dissolved in RNAse-free water and quantified by a spectrophotometer. The cDNA was synthesized using the High Capacity cDNA Reverse Transcription Kit (Applied Biosystems, Foster City, CA).

Real-time RT-PCR. mRNA expression levels of TNF-α, IL-6, IL-10, Cox-2 and human AM were measured by quantitative real-time RT-PCR based on TaqMan chemistry (Applied Biosystems) using an ABI PRISM 7700 sequence detector (Applied Biosystems). The reaction mixture contained 0.5 μl of 5 μmol/l probe (final concentration, 100 nmol/l); 1 μl of 10 μmol/l forward primer and 1 μl of 10 μmol/l reverse primer (400 nmol/l final concentration of each primer); 12.5 μl of TaqMan Universal Mastermix, 5 μl of diethyl pyrocarbonate–treated water, and 5 μl of a cDNA sample. Assay controls were performed in the same TaqMan plate with no-template controls to test for the contamination of any assay reagents. The thermocycling conditions were initiated at 50 °C for 2 minutes with an enzyme activation step of 95 °C for 10 minutes followed by 40 PCR cycles of denaturation at 95 °C for 15 seconds, and anneal/extension at 60 °C for 1 minute.

Hemodynamic studies. Hemodynamic studies were performed 4 weeks after gene transfer. Rats were anesthetized with intraperitoneal pentobarbital (30 mg/kg) and placed on a heating pad to maintain body temperature 37–38 °C throughout the study. Under sterile conditions, a polyethylene catheter (PE-50; BD Biosciences, San Jose, CA) was inserted through the right jugular vein into the right ventricle to measure right ventricular pressure by a hemodynamic transducer (PowerLab 8/30; ADInstruments, Colorado Springs, CO).

Evaluation of gene transfer effect in a PAH rat model. Monocrotaline (60 mg/kg) was subcutaneously injected into male Wistar rats and left for 4 weeks to make a model of PAH. After 4 weeks, a hemodynamic study was performed to introduce a catheter into the right ventricle through the right jugular vein. The PEG-*b*-P[Asp(DET)] polyplex nanomicelle loaded with the AM expression vector (200 μg of DNA for each rat) in a 200 μl of solution was sprayed intratracheally. Three days later, a hemodynamic study was performed again and the gene transfer effect was evaluated. Pulmonary tissue specimens were frozen to measure *AM* gene expression by real-time RT-PCR.

Statistical analysis. All data are expressed as means ± SEM unless otherwise indicated. Comparisons of parameters among four groups were made by one-way analysis of variance, followed by Scheffe's multiple-comparison test. Paired *t*-test was applied for the comparison of the values before and after the gene transfection (**Figure 7**).

SUPPLEMENTARY MATERIAL

Figure S1. The restriction maps of expression vector for luciferase and human adrenomedullin cDNA.

ACKNOWLEDGMENTS

This work was supported by the Core Research Program for Evolutional Science and Technology from the Japan Science and Technology

Corporation, by Grants-in-Aid for Scientific Research from the Japanese Ministry of Health, Labor, and Welfare (H19-Nano-012 and H20-Genomu-Ippan-008), by the Program for the Promotion of Fundamental Studies in Health Sciences of the National Institute of Biomedical Innovation of Japan, and by the Takeda Science Foundation. We thank Keiko Jinno, Shoko Obora, Hiroko Miyata, Moto Ohira, and Eri Abe and Mutsumi Goda (National Cardiovascular Center Research Institute) for their excellent technical assistance, including animal care. We also thank Hisayuki Matsuo and Hitonobu Tomoike for their helpful discussion and advice, Darin Y. Furgeson (University of Wisconsin–Madison) for proofreading of this manuscript.

REFERENCES

1. Rubin, LJ (2006). Pulmonary arterial hypertension. *Proc Am Thorac Soc* **3**: 111–115.
2. Badesch, DB, Abman, SH, Ahearn, GS, Barst, RJ, McCrory, DC, Simonneau, G *et al.* (2004). Medical therapy for pulmonary arterial hypertension: ACCP evidence-based clinical practice guidelines. *Chest* **126**(1 Suppl): 35S–62S.
3. D'Alonzo, GE, Barst, RJ, Ayres, SM, Bergofsky, EH, Brundage, BH, Detre, KM *et al.* (1991). Survival in patients with primary pulmonary hypertension. Results from a national prospective registry. *Ann Intern Med* **115**: 343–349.
4. Kitamura, K, Kangawa, K, Kawamoto, M, Ichiki, Y, Nakamura, S, Matsuo, H *et al.* (1993). Adrenomedullin: a novel hypotensive peptide isolated from human pheochromocytoma. *Biochem Biophys Res Commun* **192**: 553–560.
5. Kitamura, K, Kangawa, K and Eto, T (2002). Adrenomedullin and PAMP: discovery, structures, and cardiovascular functions. *Microsc Res Tech* **57**: 3–13.
6. Nagaya, N, Mori, H, Murakami, S, Kangawa, K and Kitamura, S (2005). Adrenomedullin: angiogenesis and gene therapy. *Am J Physiol Regul Integr Comp Physiol* **288**: R1432–R1437.
7. Nagaya, N, Okumura, H, Uematsu, M, Shimizu, W, Ono, F, Shirai, M *et al.* (2003). Repeated inhalation of adrenomedullin ameliorates pulmonary hypertension and survival in monocrotaline rats. *Am J Physiol Heart Circ Physiol* **285**: H2125–H2131.
8. Nagaya, N, Kyotani, S, Uematsu, M, Ueno, K, Oya, H, Nakanishi, N *et al.* (2004). Effects of adrenomedullin inhalation on hemodynamics and exercise capacity in patients with idiopathic pulmonary arterial hypertension. *Circulation* **109**: 351–356.
9. Katayose, S and Kataoka, K (1997). Water-soluble polyion complex associates of DNA and poly(ethylene glycol)-poly(L-lysine) block copolymer. *Bioconjug Chem* **8**: 702–707.
10. Kakizawa, Y and Kataoka, K (2002). Block copolymer micelles for delivery of gene and related compounds. *Adv Drug Deliv Rev* **54**: 203–222.
11. Katayose, S and Kataoka, K (1998). Remarkable increase in nuclease resistance of plasmid DNA through supramolecular assembly with poly(ethylene glycol)-poly(L-lysine) block copolymer. *J Pharm Sci* **87**: 160–163.
12. Itaka, K, Yamauchi, K, Harada, A, Nakamura, K, Kawaguchi, H and Kataoka, K (2003). Polyion complex micelles from plasmid DNA and poly(ethylene glycol)-poly(L-lysine) block copolymer as serum-tolerable polyplex system: physicochemical properties of micelles relevant to gene transfection efficiency. *Biomaterials* **24**: 4495–4506.
13. Harada-Shiba, M, Yamauchi, K, Harada, A, Takamisawa, I, Shimokado, K and Kataoka, K (2002). Polyion complex micelles as vectors in gene therapy—pharmacokinetics and *in vivo* gene transfer. *Gene Ther* **9**: 407–414.
14. Kanayama, N, Fukushima, S, Nishiyama, N, Itaka, K, Jang, WD, Miyata, K *et al.* (2006). A PEG-based biocompatible block catiomer with high buffering capacity for the construction of polyplex micelles showing efficient gene transfer toward primary cells. *ChemMedChem* **1**: 439–444.
15. Itaka, K, Ohba, S, Miyata, K, Kawaguchi, H, Nakamura, K, Takato, T *et al.* (2007). Bone regeneration by regulated *in vivo* gene transfer using biocompatible polyplex nanomicelles. *Mol Ther* **15**: 1655–1662.
16. Akagi, D, Oba, M, Koyama, H, Nishiyama, N, Fukushima, S, Miyata, T *et al.* (2007). Biocompatible micellar nanovectors achieve efficient gene transfer to vascular lesions without cytotoxicity and thrombus formation. *Gene Ther* **14**: 1029–1038.
17. Nossaman, BD, Gur, S and Kadowitz, PJ (2007). Gene and stem cell therapy in the treatment of erectile dysfunction and pulmonary hypertension; potential treatments for the common problem of endothelial dysfunction. *Curr Gene Ther* **7**: 131–153.
18. Champion, HC, Bivalacqua, TJ, Greenberg, SS, Giles, TD, Hyman, AL, Kadowitz, PJ (2002). Adenoviral gene transfer of endothelial nitric-oxide synthase (eNOS) partially restores normal pulmonary arterial pressure in eNOS-deficient mice. *Proc Natl Acad Sci USA* **99**: 13248–13253.
19. Champion, HC, Bivalacqua, TJ, Toyoda, K, Heistad, DD, Hyman, AL and Kadowitz, PJ (2000). *In vivo* gene transfer of prepro-calcitonin gene-related peptide to the lung attenuates chronic hypoxia-induced pulmonary hypertension in the mouse. *Circulation* **101**: 923–930.
20. Nagaya, N, Yokoyama, C, Kyotani, S, Shimonishi, M, Morishita, R, Uematsu, M *et al.* (2000). Gene transfer of human prostacyclin synthase ameliorates monocrotaline-induced pulmonary hypertension in rats. *Circulation* **102**: 2005–2010.
21. Masago, K, Itaka, K, Nishiyama, N, Chung, UI and Kataoka, K (2007). Gene delivery with biocompatible cationic polymer: Pharmacogenomic analysis on cell bioactivity. *Biomaterials* **28**: 5169–5175.
22. Miyata, K, Oba, M, Nakanishi, M, Fukushima, S, Yamasaki, Y, Koyama, H *et al.* (2008). Polyplexes from poly(aspartamide) bearing 1,2-diaminoethane side chains induce pH-selective, endosomal membrane destabilization with amplified transfection and negligible cytotoxicity. *J Am Chem Soc* **130**: 16287–16294.
23. Bragonzi, A, Dina, G, Villa, A, Calori, G, Biffi, A, Bordignon, C *et al.* (2000). Biodistribution and transgene expression with nonviral cationic vector/DNA complexes in the lungs. *Gene Ther* **7**: 1753–1760.
24. Wiseman, JW, Goddard, CA, McLelland, D and Colledge, WH (2003). A comparison of linear and branched polyethylenimine (PEI) with DCChol/DOPE liposomes for gene delivery to epithelial cells *in vitro* and *in vivo*. *Gene Ther* **10**: 1654–1662.
25. Kim, TW, Chung, H, Kwon, IC, Sung, HC, Shin, BC and Jeong, SY (2005). Airway gene transfer using cationic emulsion as a mucosal gene carrier. *J Gene Med* **7**: 749–758.
26. Densmore, CL (2006). Advances in noninvasive pulmonary gene therapy. *Curr Drug Deliv* **3**: 55–63.
27. Furgeson, DY, Chan, WS, Yockman, JW and Kim, SW (2003). Modified linear polyethylenimine-cholesterol conjugates for DNA complexation. *Bioconjug Chem* **14**: 840–847.
28. Gautam, A, Densmore, CL and Waldrep, JC (2001). Pulmonary cytokine responses associated with PEI-DNA aerosol gene therapy. *Gene Ther* **8**: 254–257.
29. Regnstrom, K, Ragnarsson, EG, Koping-Hoggard, M, Torstensson, E, Nyblom, H and Artursson, P (2003). PEI—a potent, but not harmless, mucosal immuno-stimulator of mixed T-helper cell response and FasL-mediated cell death in mice. *Gene Ther* **10**: 1575–1583.
30. Budts, W, Pokreisz, P, Nong, Z, Van Pelt, N, Gillijns, H, Gerard, R *et al.* (2000). Aerosol gene transfer with inducible nitric oxide synthase reduces hypoxic pulmonary hypertension and pulmonary vascular remodeling in rats. *Circulation* **102**: 2880–2885.
31. Chicoine, LG, Tzeng, E, Bryan, R, Saenz, S, Paffett, ML, Jones, J *et al.* (2004). Intratracheal adenoviral-mediated delivery of iNOS decreases pulmonary vasoconstrictor responses in rats. *J Appl Physiol* **97**: 1814–1822.
32. Campbell, AI, Zhao, Y, Sandhu, R and Stewart, DJ (2001). Cell-based gene transfer of vascular endothelial growth factor attenuates monocrotaline-induced pulmonary hypertension. *Circulation* **104**: 2242–2248.
33. Gong, F, Tang, H, Lin, Y, Gu, W, Wang, W and Kang, M (2005). Gene transfer of vascular endothelial growth factor reduces bleomycin-induced pulmonary hypertension in immature rabbits. *Pediatr Int* **47**: 242–247.
34. Suhara, H, Sawa, Y, Fukushima, N, Kagisaki, K, Yokoyama, C, Tanabe, T *et al.* (2002). Gene transfer of human prostacyclin synthase into the liver is effective for the treatment of pulmonary hypertension in rats. *J Thorac Cardiovasc Surg* **123**: 855–861.
35. Ono, M, Sawa, Y, Fukushima, N, Suhara, H, Nakamura, T, Yokoyama, C *et al.* (2004). Gene transfer of hepatocyte growth factor with prostacyclin synthase in severe pulmonary hypertension of rats. *Eur J Cardiothorac Surg* **26**: 1092–1097.
36. Ono, M, Sawa, Y, Mizuno, S, Fukushima, N, Ichikawa, H, Bessho, K *et al.* (2004). Hepatocyte growth factor suppresses vascular medial hyperplasia and matrix accumulation in advanced pulmonary hypertension of rats. *Circulation* **110**: 2896–2902.
37. Lippton, H, Chang, JK, Hao, Q, Summer, W and Hyman, AL (1994). Adrenomedullin dilates the pulmonary vascular bed *in vivo*. *J Appl Physiol* **76**: 2154–2156.
38. Ishizaka, Y, Ishizaka, Y, Tanaka, M, Kitamura, K, Kangawa, K, Minamino, N *et al.* (1994). Adrenomedullin stimulates cyclic AMP formation in rat vascular smooth muscle cells. *Biochem Biophys Res Commun* **200**: 642–646.
39. Kakishita, M, Nishikimi, T, Okano, Y, Satoh, T, Kyotani, S, Nagaya, N *et al.* (1999). Increased plasma levels of adrenomedullin in patients with pulmonary hypertension. *Clin Sci (Lond)* **96**: 33–39.
40. Yoshibayashi, M, Kamiya, T, Kitamura, K, Saito, Y, Kangawa, K, Nishikimi, T *et al.* (1997). Plasma levels of adrenomedullin in primary and secondary pulmonary hypertension in patients <20 years of age. *Am J Cardiol* **79**: 1556–1558.
41. Nagaya, N, Nishikimi, T, Uematsu, M, Satoh, T, Oya, H, Kyotani, S *et al.* (2000). Haemodynamic and hormonal effects of adrenomedullin in patients with pulmonary hypertension. *Heart* **84**: 653–658.
42. Kitamura, K, Sakata, J, Kangawa, K, Kojima, M, Matsuo, H and Eto, T (1993). Cloning and characterization of cDNA encoding a precursor for human adrenomedullin. *Biochem Biophys Res Commun* **194**: 720–725.
43. de Wet, JR, Wood, KV, DeLuca, M, Helinski, DR and Subramani, S (1987). Firefly luciferase gene: structure and expression in mammalian cells. *Mol Cell Biol* **7**: 725–737.

In Vivo Tissue Response and Degradation Behavior of PLLA and Stereocomplexed PLA Nanofibers

Daisuke Ishii,[†,‡] Tang Hui Ying,[†,§,||] Atsushi Mahara,[⊥] Sunao Murakami,[⊥] Tetsuji Yamaoka,[⊥] Won-ki Lee,[▽] and Tadahisa Iwata*[,†,○]

Polymer Chemistry Laboratory, RIKEN Institute, 2-1 Hirosawa, Wako-shi, Saitama 351-0198, Japan, School of Biological Science, Universiti Sains Malaysia, 11800 Penang, Malaysia, Department of Biomedical Engineering, Advanced Medical Engineering Center, National Cardiovascular Center Research Institute, 5-7-1 Fujishirodai, Suita, Osaka 565-8565, Japan, and Division of Chemical Engineering, Pukyong National University, San 100, Yongdang-dong, Nam-gu, Busan 608-739, Republic of Korea

Received August 21, 2008; Revised Manuscript Received November 24, 2008

Biocompatibility of PLLA and stereocomplexed PLA nanofibers was evaluated by subcutaneous implantation in rats for 4−12 weeks. Characterization of the nanofibers was performed by GPC, SEM, wide-angle X-ray diffraction, and optical microscopy of hematoxylin-eosin stained ultrathin sections of explanted nanofibers. Stereocomplexed PLA nanofiber showed slower degradation than PLLA nanofiber and thus retained their shape after prolonged implantation. Furthermore, stereocomplexed PLA nanofiber caused milder inflammatory reaction than PLLA nanofiber. These results offer the potential use of PLLA and stereocomplexed PLA nanofibers as a biomaterial for short-term and long-term tissue regeneration, respectively. Stereocomplexed PLA nanofiber after in vitro degradation showed smaller degree of swelling than PLLA nanofiber. Taking the results of in vivo degradation together with in vitro degradation into consideration, bioabsorption mechanism of the in vivo degradation of the nanofibers is proposed.

Introduction

In the field of medical sciences, the method of tissue engineering has been extensively studied to overcome the problems of conventional methods such as organ transplantation and usage of artificial organs.[1] In tissue engineering, the proliferation and differentiation of cultured cells for deficiency repair has to be artificially controlled. The development of scaffold materials on which cells proliferate and differentiate has been a major concern in tissue engineering. Conventionally, collagens and gelatins extracted from animals have been used to produce scaffolds. However, the usage of these animal-origin materials is shrinking for fear of infectious diseases. Alternatively, the usage of biodegradable and biocompatible polymers that do not contain infectious substances such as endotoxins and prions has been explored.

Recently, as a novel method for producing scaffolds, formation of nanofibers with the diameter ranging from several tens to hundreds of nanometers is extensively studied.[2−4] Nanofiber scaffolds have fine pores and grooves as small as a few micrometers wide. Such fine structural features facilitate the adhesion and proliferation of cells. It is required for nanofiber scaffolds to sustain sufficient strength to support regenerating tissue cells and to be degraded after the tissue regeneration is completed. To meet these demands, various kinds of biodegradable and biocompatible polymers have been processed into nanofibers. Furthermore, the fiber morphology, crystalline structure, and degradation behavior of the nanofibers have been investigated.[5−7]

Poly(lactide) (PLA) is one of a few polymers that is practically applied as various medical materials such as implants and sutures.[8] PLA possesses mechanical properties sufficient to endure the mechanical load applied in human body. However, it is readily hydrolyzed both in enzymatic and nonenzymatic conditions.[9] The high susceptibility of PLA toward hydrolysis becomes a shortcoming when the long-time storage under physiological conditions is required. Various efforts to overcome this shortcoming have been attempted. One of such efforts is the formation of stereocomplex in PLA materials.

Stereocomplexed PLA is a characteristic crystalline form of PLA.[10,11] A sterically stable racemic crystal of stereocomplexed PLA is formed by complexing poly(L-lactide) (PLLA) and poly(D-lactide) (PDLA) that take molecular conformations of left-handed and right-handed helices, respectively.[12] As a result, stereocomplexed PLA has a melting temperature of 230 °C, that is 50 °C higher than PLLA and PDLA.[10] Furthermore, it has been reported that stereocomplexed PLA is more stable against hydrolysis than PLLA.[13−15] This finding offers the possibility for controlling the hydrolytic behavior of PLA material by the formation of stereocomplex. Although various methods have been proposed and investigated for the formation of stereocomplex within PLA materials,[16,17] PLA materials that contain only racemic crystal has not yet been processed. Furthermore, the conventional processes involve long-time annealing at elevated temperatures as high as 180 °C and repeated stretching. To form stereocomplexed PLA more conveniently, electrospinning has recently been applied to the formation of stereocomplexed

* To whom correspondence should be addressed. Tel.: +81-3-5841-7888. Fax: +81-3-5841-1304. E-mail: atiwata@mail.ecc.u-tokyo.ac.jp.
† RIKEN Institute.
‡ Present affiliation and address: Department of Materials Chemistry, Faculty of Science and Technology, Ryukoku University 1-5 Yokotani, Seta Oe-cho, Otsu-shi, Shiga 520-2194, Japan.
§ Universiti Sains Malaysia.
|| Present affiliation and address: Bioengineering Laboratory, RIKEN Institute, 2-1 Hirosawa, Wako-shi, Saitama 351-0198, Japan.
⊥ National Cardiovascular Center Research Institute.
▽ Pukyong National University.
○ Present affiliation and address: Graduate School of Agricultural and Life Sciences, The University of Tokyo, 1-1-1 Yayoi, Bunkyo-ku, Tokyo 113-8657, Japan.

10.1021/bm8009363 CCC: $40.75
Published on Web 12/31/2008

PLA.[18] In particular, we have first succeeded in processing sterecomplexed PLA nanofiber in which the racemic crystal is only the crystalline polymorph.[19] The formation of racemic crystal was performed by annealing the as-spun nanofiber at 100 °C, which is 80 °C lower than those in previously reported studies.

The degradation behavior of PLA nanofibers has been investigated by using various specimens and conditions.[20−22] However, the previous reports were all limited to in vitro conditions. There have been no reports on the biocompatibility and in vivo degradation behavior of stereocomplexed PLA nanofibers.

In this work, tissue responses and degradation behavior of PLLA and stereocomplexed PLA nanofibers in vivo were investigated by subcutaneously implanting these nanofibers in rats. The tissue response against the nanofibers has been investigated by means of histological observation. The changes in structure and properties of the nanofibers during subcutaneous implantation has been investigated using scanning electron microscopy (SEM), wide-angle X-ray diffraction (WAXD), gel permeation chromatography (GPC), and mechanical tensile testing. The relation between tissue response and degradation behavior of nanofibers is discussed in terms of the structural and property changes of the nanofibers.

Experimental Section

Materials. PLLA with a M_n of 4.7×10^5 and M_w/M_n of 1.8 was purchased from Polysciences, Inc. and used as received. PDLA with a $M_n = 2.2 \times 10^5$ and M_w/M_n of 1.5 was synthesized according to the following procedure. The D-lactide monomer, obtained from Purac, was recrystallized from anhydrous ethyl acetate. Bulk polymerizations were carried out in glass ampoules containing a magnetic stirring bar at 130 °C. Stannous octanoate in petroleum ether was used as the catalyst for the ring-opening polymerization. The ampoules were evacuated using a high vacuum pump and repeatedly flushed with high purity nitrogen to remove volatile impurities, solvents, and oxygen. Then the ampoules were sealed with a blowtorch and heated to the reaction temperature. The products in the ampoules were dissolved in chloroform, precipitated in the excess of methanol, filtered, and dried.

Electrospinning. Solutions of PLLA and PDLA (1 wt %) were prepared using 1,1,1,3,3,3-hexafluoro-2-propanol, HFIP, as the solvent. For the preparation of PLA stereocomplex nanofibers, equal volume of PLLA and PDLA solutions were mixed for several seconds by vortex mixer. Nanofibers were prepared using an Esprayer ES-2000 electrospinning device by Fuence, Co. Ltd. Dope solutions were extruded with a speed of 2.4 mL/h from a syringe needle with an inner diameter of 0.5 mm. Electrical voltage of 15 kV was applied to the syringe. Nanofibers were deposited onto a 10×10 cm^2 aluminum substrate placed perpendicular to the needle. To ensure sufficient thickness of nanofiber mats, the substrate was covered with a template made by a 51.4 μm thick Kapton film on which a 3×3 cm^2 window was opened. Distance between the needle tip and the substrate was set to 15 cm. The atmosphere of the spinning chamber was kept at less than 30% of relative humidity. PLLA and PLA stereocomplex nanofibers were then annealed in an oven at 100 °C for 8 h. Each electrospun PLA nanofiber mats was then cut into two different dimensions measuring 1×1 cm^2 and 1×3 cm^2, respectively. To prevent contamination, all scaffolds were sterilized overnight with ethylene oxide at 40 °C and kept in sealed bags until use.

Subcutaneous Implantation in Rat and Retrieval. Two 12-week old male Wistar rats were used for implanting the scaffolds; one for scaffolds measuring 1×1 cm^2, while the other for scaffolds measuring 1×3 cm^2. The experimental protocol had been approved by the Animal Care Committee of the National Cardiovascular Center, Osaka, Japan. The implantation of nanofiber mat was performed under anesthesia using diethyl ether. The 1×1 cm^2 scaffolds were implanted subcutaneously at one side of the backbone while the 1×3 cm^2 scaffolds were implanted subcutaneously at the backbone. The grouping of the rats was based on the duration of observation for 4 weeks and 12 weeks.

Upon explantation, the nanofiber mats measuring 1×1 cm^2 were excised with the surrounding tissues and stored in 2.5% glutaraldehyde in phosphate buffer saline (PBS) with a pH of 7 until further preparation of ultrathin section for histological observation. The retrieved 1×3 cm^2 nanofiber mats were treated with 1.25 wt % trypsin solution to remove the surrounding tissues. They were then kept in tubes containing PBS at 4 °C until further use. Trace amount of sodium azide was added to avoid the decay of the specimens. After trypsin treatment, surrounding tissues were manually removed as much as possible. The nanofiber mats were repeatedly washed using milli-Q water and dehydrated using ethanol series. Finally, the dehydrated nanofiber mats were dried overnight using vacuum desiccator at room temperature.

In Vitro Degradation. Nanofiber mats with the size of 1×3 cm^2 were incubated in 5 mL of PBS with a pH of 7.27 for 4−12 weeks at 37 °C. The medium was changed every 2 weeks. After 4 and 12 weeks of incubation, the nanofiber mats were washed thoroughly with distilled water, vacuum-dried at room temperature, and then subjected to SEM observation.

Histological Observation. The surrounding tissues were excised together with the implanted nanofiber mats and fixed with 2.5% glutaraldehyde in PBS with a pH of 7. A small piece of the tissue was then embedded in paraffin before subjecting it to microtome sectioning. Hematoxylin and eosin (HE) were used for staining the tissues. The tissue response to nanofiber mats was evaluated from the coloration observed with a phase-contrast microscope.

Scanning Electron Microscopy (SEM). Nanofiber mat was placed on a stub and then coated with Au. The thickness of Au coat was about 15 nm. SEM images of nanofibers were obtained using a field emission scanning electron microspope (JSM-6330F, JEOL, Co. Ltd.) operating at an acceleration voltage of 5 kV of and an emission current of 12 μA. For estimating the average diameter of nanofibers, diameter was measured at more than 60 points on the printed SEM image.

Wide-Angle X-ray Diffraction (WAXD). WAXD patterns of nanofiber mats were acquired under ambient condition using Rigaku RINT-2500 system operating at 40 kV and 200 mA. Measurements were performed on a Bragg−Brentano type $2\theta/\theta$ goniometer in a reflection mode. Ni-filtered Cu Kα radiation ($\lambda = 0.15418$ nm) was collimated with a 1/2 deg divergence slit, 1/6 deg scatter slit and 0.15 mm receiving slit. Scans were performed three times in a 2θ range of 10−40° with a scan rate of 0.5°/min and 0.05° step.

Gel Permeation Chromatography (GPC) Analysis. The molecular weight analysis of the nanofiber mats was performed with gel-permeation chromatography at 40 °C, using a Shimadzu LC-10A GPC system equipped with a RID-10A refractive index detector and Shodex K-806 M and K-802 columns. Chloroform was used as the eluent at a flow rate of 0.8 mL min^{-1}. The calibration curve was prepared by using monodisperse polystyrene standards.

Results

Changes in the Appearance of Nanofiber Mats During Subcutaneous Implantation. Figure 1a,b shows SEM images of the PLLA and stereocomplexed PLA nanofibers, respectively. Both nanofibers possess similar morphology with the average fiber diameter of about 300 nm. However, totally different crystalline structure is formed in these nanofibers, as seen from the WAXD profiles in Figure 1c. PLLA nanofiber shows diffraction peaks at $2\theta = 15.1$, 16.5 (assigned to (110)/(200)), and 18.1° that are assigned to α-form homocrystal of PLA.[12] On the other hand, stereocomplexed PLA nanofiber showed diffraction peaks at $2\theta = 12.0$ (assigned to (110)), 20.8, and 24.1° that are assigned only to stereocomplex crystal of PLA.[12]

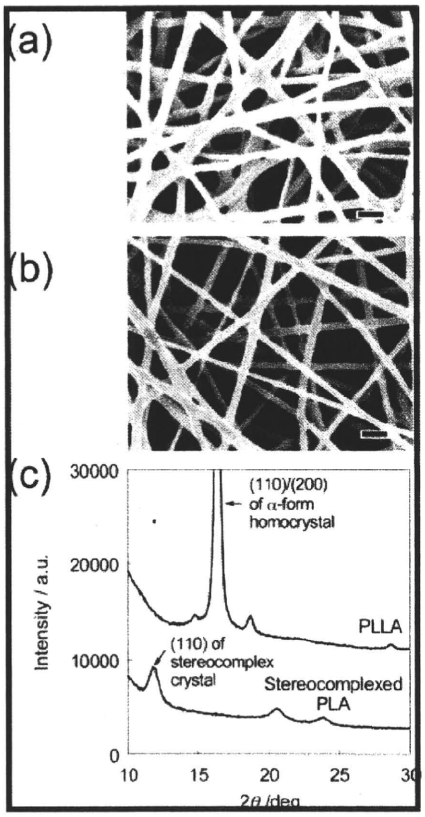

Figure 1. SEM images of (a) PLLA and (b) stereocomplexed PLA nanifibers and (c) wide-angle X-day diffraction patterns of PLLA and stereocomplexed PLA nanofibers. Scale bars = 1 μm. PLLA nanofiber shows diffraction peaks at 2θ = 15.1, 16.5 (assigned to (110)/(200)), and 18.1° that are assigned to α-form homocrystal of PLA. On the other hand, stereocomplexed PLA nanofiber showed diffraction peaks at 2θ = 12.0 (assigned to (110)), 20.8, and 24.1° that are aasigned only to stereocomplex crystal of PLA.

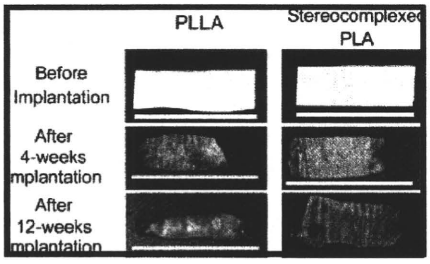

Figure 2. Bulk appearances of the nanofiber mats of PLLA and stereocomplexed PLA (a) before implantation, (b) after 4 weeks of implantation and (c) after 12 weeks of implantation. Scale bars = 3 cm.

This shows that the stereocomplexed PLA nanofiber consists of only the stereocomplex crystal and does not contain homocrystal of PLLA and PDLA at all.

The bulk appearances of the nanofiber mats were observed before and after removing the surrounding tissues. Figure 2 shows the photographs of nanofiber mats before and after 4 week and 12 week implantations, respectively. Significant reduction in the size of the PLLA nanofiber mat was recognized with the increasing period of implantation. In particular, the PLLA nanofiber mat after a 12 week implantation was densely covered with the surrounding tissues and only small fragments of the nanofibers mat were recovered. On the other hand, the stereocomplexed PLA nanofiber mat showed a less degree of the reduction in size than the PLLA nanofiber mat. This suggests

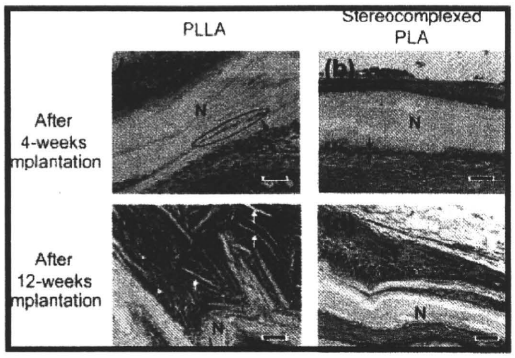

Figure 3. Histological images of PLLA and stereocomplexed PLA nanofibers before and after 4 weeks of implantation. (a) PLLA, before implantation; (b) stereocomplexed PLA, before implantation; (c) PLLA, after implantation; (d) stereocomplexed PLA, after implantation. Tissues were stained with hematoxylineosin. Nuclei of the inflammatory cells are stained blue. The width of inflammatory cells is indicated by the arrows and lines in (a) and (b). Ellipsoid region in (a) and white arrows in (c) indicate the infiltration of surrounding tissues and fragmented nanofibers, respectively. ST: surrounding tissues; N: nanofiber mats. Scale bars = 50 μm.

that the in vivo degradation of the stereocomplexed PLA nanofiber mat occurs slower than the PLLA nanofiber mat.

Histological Observation of Nanofiber Mats with the Surrounding Tissues. Histological observations of the nanofiber mats were performed to investigate the degree of inflammatory reactions and penetration of the surrounding tissues into the nanofiber mats. Figure 3 shows the phase contrast images of ultrathin sections of the explanted nanofiber mats stained by hematoxylin-eosin. The nuclei of inflammatory cells were stained blue by the hematoxylin dye and their presence is an indication of tissue response toward the implanted nanofiber mats. As indicated by the arrows and lines in Figure 3a, a thick layer of inflammatory cells was accumulated at the interface between the PLLA nanofiber mat and the surrounding tissues. In contrast, the layer of accumulated inflammatory cells was thinner for the stereocomplexed PLA nanofiber mat, as shown in Figure 3b. This indicates that the stereocomplexed PLA nanofiber mat causes smaller degree of inflammatory reactions than the PLLA nanofiber mat.

Furthermore, delamination (indicated by the ellipsoid in Figure 3a) occurred on the surface of the PLLA nanofiber mat, and hence, the infiltration of the surrounding tissues was observed. However, no infiltration of the surrounding tissues was observed for the stereocomplexed PLA nanofiber mat. After 12 weeks of implantation, while the PLLA nanofiber mat was significantly fragmented (white arrows indicate the fragmented nanofiber mat), the stereocomplexed PLA nanofibers retained the mat-like bulk morphology. These trends are well correlated with the bulk appearances of the nanofiber mats and support the observation that the in vivo degradation of the stereocomplexed PLA nanofiber mat proceeds slower than the PLLA nanofiber mat.

SEM Observation. SEM observation was performed for the nanofiber mats before and after 4 weeks and 12 weeks of implantation. Figure 4 shows the SEM images of nanofiber mats before implantation, after implantation and incubation at different periods of time. As for PLLA, cleavage of each strand of nanofiber occurred after 4 weeks. Furthermore, after 12 weeks, a decrease in the density of the nanofiber mat was observed. This is consistent with the histological image showing the fragmentation of the PLLA nanofiber mat. On the other hand, no cleavage of the stereocomplexed PLA nanofibers was observed even after 12 weeks of implantation.

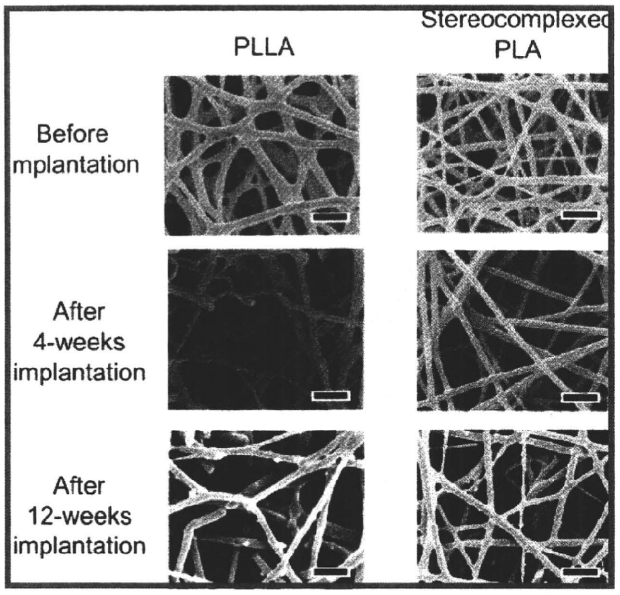

Figure 4. SEM images of PLLA (left) and stereocomplexed PLA (right) nanofibers. Upper row, before implantation; middle row, after 4 weeks of implantation; lower row, after 12 weeks of implantation. The surrounding tissues were removed by trypsin treatment. Scale bars = 1 μm.

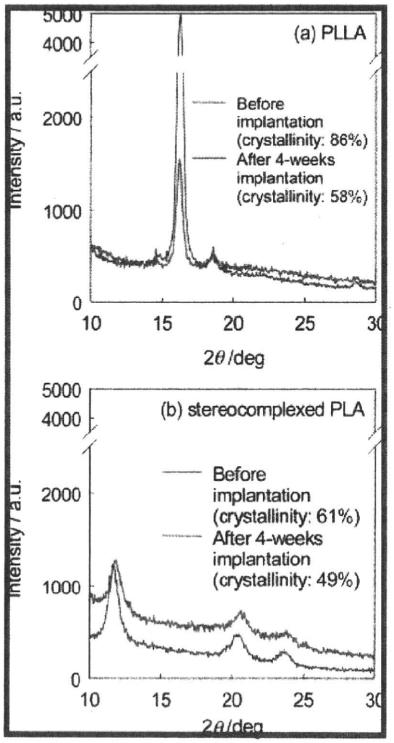

Figure 5. Wide-angle X-ray diffraction patterns of PLLA and stereocomplexed nanofibers before and after 4 weeks of implantation. PLLA nanofiber showed diffraction peaks at 2θ = 15.1°, 16.5°, and 18.1° that are assigned to homopolymer crystal of PLLA. On the other hand, stereocomplexed PLA nanofiber showed diffraction peaks at 2θ = 12.0, 20.8, and 24.1° that are assigned to stereocomplexed crystal. No diffraction peaks assigned to homopolymer crystal were observed in stereocomplexed PLA nanofiber.

Changes in Crystallinity. Figure 5 shows the WAXD patterns of the PLLA and stereocomplexed PLA nanofibers before and after 4 weeks of implantation. While the PLLA nanofiber showed diffractions that are assigned to the α-form crystal of PLA, the stereocomplexed PLA nanofiber showed diffractions assigned only to stereocomplexed crystal.[12] The crystallinity of both nanofibers was calculated as the ratio between the integrals of crystalline diffraction intensity and the total diffraction intensity. While the PLLA nanofiber showed considerable decrease in its crystallinity from 86 to 58%, the stereocomplexed PLA nanofiber showed a smaller decrease from 61 to 49%. These results show that the crystallinity of the stereocomplexed PLA is not so much lowered by implantation, while that of PLLA nanofiber significantly decreases. These results support the higher stability of stereocomplexed PLA nanofiber than PLLA nanofiber, as seen from visual inspection of the explanted nanofiber mat and the histological observation.

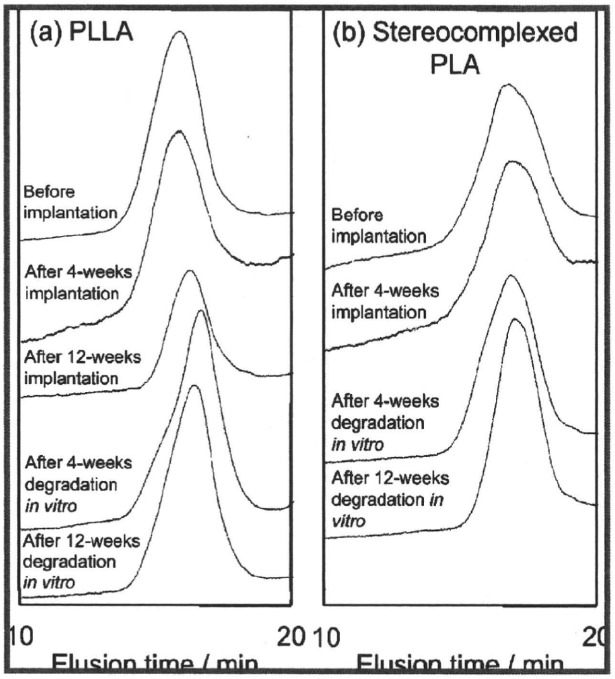

Figure 6. GPC elusion profiles of (a) PLLA and (b) stereocomplexed PLA nanofibers before and after implantation in vivo for 4 weeks and 12 weeks and before and after in vitro degradation for 4 weeks and 12 weeks.

GPC Analysis. The possibility of the cleavage of molecular chains during implantation, as suggested from SEM and WAXD data, was investigated by GPC analysis. The GPC elusion profiles are shown in Figure 6. Table 1 shows the number-averaged molecular weight, M_n, and the polydispersity index, M_w/M_n, of the PLLA and stereocomplexed PLA nanofibers before and after 4 weeks of implantation. Data for original PLLA are slso shown in Table 1. In the case of 12 weeks, GPC data of stereocomplexed PLA were not obtained because of its low solubility in chloroform. PLLA nanofiber showed a decrease in M_n during the implantation. In contrast, the M_n of stereocomplexed PLA nanofiber remained unchanged despite the decrease in M_w/M_n for 4 weeks of implantation. These results indicate that stereocomplexed PLA was not degradaded during implantation, while the PLLA chains in the nanofiber were considerably degraded. Additionally, in the case of the stereocomplexed PLA nanofiber, the extraction of low molecular weight fraction might occur during implantation.

In Vitro Degradation. To consider the results obtained from the in vivo experiment in terms of biocompatibility and bioabsorption, changes in the structure and properties of the nanofibers after in vitro incubation were investigated. As seen in Figure 7, both PLLA and stereocomplexed PLA nanofibers

Table 1. Number-Averaged Molecular Weight (M_n) and Polydispersity Index (M_w/M_n) of Original PLLA and PLA Nanofibers[a]

	PLLA		PDLA		stereocomplexed PLA	
	M_n	M_w/M_n	M_n	M_w/M_n	M_n	M_w/M_n
original	4.7×10^5	1.8	2.2×10^5	1.5		
nanofiber before implantation	3.8×10^5	2.3			8.7×10^4	3.3
after 4 weeks of implantation	3.0×10^5	2.4			8.6×10^4	2.3
after 12 weeks of implantation	1.7×10^5	2.3			[b]	[b]

[a] PLLA and stereocomplexed PLA before and after 4 weeks and 12 weeks of implantation. [b] Not obtained due to the poor solubility in chloroform.

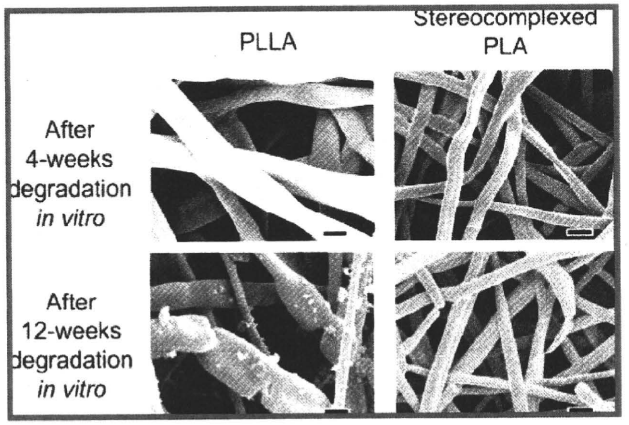

Figure 7. SEM images of PLLA (left) and stereocomplexed PLA (right) nanofibers after 4 weeks (upper) and 12 weeks (lower) in vitro degradation in PBS. Scale bars = 1 μm.

after in vitro incubation showed a considerable increase in the fiber diameter. This suggests that the significant swelling of the nanofibers occurred during the incubation. Interestingly, the stereocomplexed PLA nanofiber showed a smaller degree of swelling (from 300 to 600 nm) than the PLLA nanofiber (from 300 to 1200 nm). Because strong interaction works between molecular chains of PLLA and PDLA in the sterecomplexed PLA nanofiber, the swelling of the stereocomplexed PLA nanofiber might be suppressed.

GPC data of the nanofibers before and after in vitro degradation were also obtained, as shown in Figure 6b. The M_n and M_w/M_n estimated from the GPC curves are listed in Table 2. The M_n of stereocomplexed PLA was almost unchanged while that of PLLA showed a decrease from 3.8×10^5 to 1.8×10^5. These trends are consistent with the molecular weight data before and after the implantation in vivo as shown in Table 1.

The difference in the swelling behavior and molecular weight change in vitro between the stereocomplexed PLA and PLLA nanofibers may explain the results of the subcutaneous implantation in vivo in which the stereocomplexed PLA nanofiber showed smaller degree of absorption than the PLLA nanofiber.

Discussion

Degradation Mechanism of PLLA and Stereocomplexed PLA Nanofibers In Vivo. A schematic representation of the degradation mechanism of the PLLA and stereocomplexed PLA nanofibers is shown in Figure 8. For the PLLA nanofiber, it is believed that the molecular chains in the amorphous region between lamella crystals are preferentially hydrolyzed due to the intracrystalline swelling. This leads to the cleavage of a nanofiber and a decrease in the molecular weight. Then the chain-end degradation at the edge of the cleaved nanofiber may occur and lead to the decrease in the crystallinity. The cleavage of nanofiber may facilitate the delamination and the subsequent fragmentation of the nanofiber mats and, consequently, the

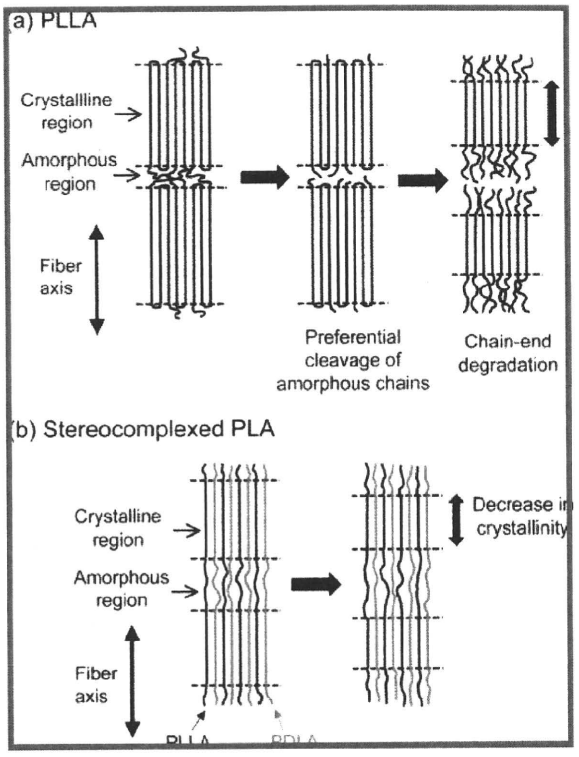

Figure 8. Schematic representation of the structural changes of (a) PLLA nanofiber and (b) stereocomplexed PLA nanofiber during implantation in vivo. For PLLA nanofiber, the amorphous chains between lamella crystals are preferentially hydrolyzed, leading to the cleavage of the nanofiber. Then, the chain-end degradation occurs at the edge of the cleaved nanofiber. Crystallinity of the PLLA nanofiber is thus considerably lowered. In contrast, degradation of stereocomplexed PLA is suppressed by the strong interaction between PLLA and PDLA chains, although the crystallinity slightly decreases.

Table 2. Number-Averaged Molecular Weight (M_n) and Polydispersity Index (M_w/M_n) of PLLA and Stereocomplexed PLA Nanofibers[a]

	PLLA		stereocomplexed PLA	
	M_n	M_w/M_n	M_n	M_w/M_n
before degradation	3.8×10^5	2.3	8.7×10^4	3.3
after 4 weeks of degradation	1.4×10^5	3.5	8.4×10^4	3.0
after 12 weeks of degradation	1.8×10^5	3.0	6.9×10^4	2.2

[a] Before and after 4 weeks and 12 weeks of degradation in vitro.

infiltration of surrounding tissues in the PLLA nanofiber mat. Inflammatory reaction at the early stage may be due to the acidic low-molecular-weight degradation products and fragmented nanofibers.

A different situation was observed for the stereocomplexed PLA nanofibers. It is supposed that a single stereocomplexed PLA nanofiber is composed of PLLA and PDLA chains aligned

in a side-by-side manner. Accordingly, it is well-known that molecular interaction between PLLA and PDLA chains is strong, leading to higher melting temperature. Such molecular arrangement may suppress the hydrolysis of molecular chains in vivo. Thus, the stereocomplexed nanofiber morphology is retained. As a result, inflammatory reaction is limited at the vicinity of the interfacial region between nanofiber mats and the surrounding tissues.

General Discussion. Physiological response of tissues against implanted foreign materials is one of the most significant subjects to be considered in the development of medical biomaterials. In the case of polymeric biomaterials, the degree of the tissue responses, such as inflammatory reactions, partly depends on the chemical structure and, as a consequence, surface hydrophilic nature of the polymers.[23] Additionally, for biodegradable polymers, the degree of tissue responses is affected by the degradability in vivo.[24] For example, poly(glycolic acid) that undergoes degradation in vivo generally in 2−4 weeks is known to cause acute inflammatory reaction as the degradation proceeds.[25] It is known that the hydrolysis by body fluids is the major mechanism contributing in vivo degradation of polymeric biomaterials. We have already shown that the degradation behavior of poly(hydroxyalkanoate)s (PHAs) in vivo are largely affected by the monomer composition.[26] Nanofiber scaffolds made from these PHAs, ranging from poly[(*R*)-3-hydroxybutyrate] to poly[(*R*)-3-hydroxybutyrate-*co*-97 mol %-4-hydroxybutyrate] lead to contrasted tissue responses. The tissue responses were well correlated with the degradability of each polymer scaffolds. The present study using nanofibers of PLLA and stereocomplexed PLA suggested the correlation between the degree of inflammatory reaction in vivo and the change in the bulk size of each nanofiber mats. The changes in bulk size of the nanofibers were correlated to the changes in the microscopic morphology, crystallinity, and molecular weight. All these factors give evidence that the stereocomplexed PLA nanofibers are more stable and thus provoke lower degree of inflammation in vivo than the PLLA nanofibers.

In general, inflammatory reaction is favored in the case where healing occurs in a short period of time. For example, inflammatory reaction stimulates and accelerates the regeneration of some kinds of epithelial tissues. On the other hand, in the case where healing requires a longer time, chronic inflammatory response is not favored. For example, suppression of the inflammatory responses against artificial vessel has significance for treatment of the circulatory organs that requires a period of more than half a year. From this viewpoint, our results show that the stereocomplexed PLA nanofibers are suitable for the purposes where the chronic inflammatory reaction should be avoided, for example, guided nerve regeneration or blood vessel augmentation. On the other hand, conventional PLLA nanofibers may be suitable for the rapidly bioresorbable materials, for example, wound healing patches. Such versatility of the biodegradability would expand the potential of PLAs as biomaterials.

Conclusion

Fiber morphology, crystallinity, and molecular weight of PLLA and stereocomplexed PLA nanofibers before and after implantation in vivo were investigated using SEM, WAXD, and GPC. The stereocomplexed PLA nanofiber retained its fiber morphology, crystallinity, and molecular weight after a 12 week implantation. On the other hand, the PLLA nanofiber showed breakdown of the fiber morphology and significant decrease in crystallinity and molecular weight. The degree of inflammatory reaction against the nanofibers in vivo was correlated to the degradation behavior. The larger stability against hydrolysis of stereocomplexed PLA nanofiber, attributed to the strong interaction between PLLA and PDLA chains in the nanofiber, was confirmed by in vitro degradation.

Acknowledgment. This work has been supported by a grant provided for Ecomolecular Research II in RIKEN Institute (The Institute of Physical and Chemical Research), Japan, and by a Grant-in-Aid from the Ministry of Education, Culture, Sports, Science and Technology, Japan (No. 19350075, to T.I.). We thank Ms. Noreen Fundador for the English correction of our manuscript.

References and Notes

(1) Langer, R.; Vacanti, J. P. *Science* **1993**, *260*, 920–926.
(2) Reneker, D. H.; Chun, I. *Nanotechnology* **1996**, *7*, 216–223.
(3) Morota, K.; Matsumoto, K.; Mizukoshi, T.; Konosu, Y.; Minagawa, M.; Tanioka, A.; Yamagata, Y.; Inoue, K. *J. Colloid Interface Sci.* **2004**, *279*, 484–492.
(4) Murugan, R.; Ramakrishna, S. *Tissue Eng.* **2006**, *12*, 435–447.
(5) Buchko, C. J.; Chen, L. C.; Shen, Y.; Martin, D. C. *Polymer* **1999**, *40*, 7397–7407.
(6) Zong, X.; Kim, K.; Fang, D.; Ran, S.; Hsiao, B. S.; Chu, B. *Polymer* **2002**, *43*, 4403–4412.
(7) Zong, X.; Ran, S.; Kim, K.-S.; Fang, D.; Hsiao, B.; Chu, B. *Biomacromolecules* **2003**, *4*, 416–423.
(8) Ikada, Y.; Tsuji, H. *Macromol. Rapid Commun.* **2000**, *21*, 117–132.
(9) Iwata, T.; Doi, Y. *Sen'i Gakkaishi* **2001**, *57*, 172–177.
(10) Ikada, Y.; Jamshidi, K.; Tsuji, H.; Hyon, S. H. *Macromolecules* **1987**, *20*, 904–906.
(11) Tsuji, H. *Macromol. Biosci.* **2005**, *5*, 569–597.
(12) Okihara, T.; Tsuji, M.; Kawaguchi, A.; Katayama, K.; Tsuji, H.; Hyon, S. H.; Ikada, Y. *J. Macromol. Sci., Part B: Phys.* **1991**, *30*, 119–140.
(13) Tsuji, H. *Polymer* **2000**, *41*, 3621–3630.
(14) Tsuji, H.; Suzuki, M. *Sen'I Gakkaishi* **2001**, *57*, 198–202.
(15) Tsuji, H.; Miyaushi, S. *Biomacromolecules* **2001**, *2*, 597–604.
(16) Takasaki, M.; Ito, H.; Kikutani, T. *J. Macromol. Sci., Part B: Phys.* **2003**, *42*, 57–73.
(17) Furuhashi, Y.; Kimura, Y.; Yamane, H. *J. Polym. Sci., Part B: Polym. Phys.* **2007**, *45*, 218–228.
(18) Tsuji, H.; Nakano, M.; Hashimoto, M.; Takashima, K.; Katsura, S.; Mizuno, A. *Biomacromolecules* **2006**, *7*, 3316–3320.
(19) Ishii, D.; Lee, W.-K.; Kasuya, K.-I.; Iwata, T. *J. Biotechnol.* **2007**, *132*, 318–324.
(20) Kim, K.; Yu, M.; Zong, X.; Chiu, J.; Fang, D.; Seo, Y.-S.; Hsiao, B. S.; Chu, B.; Hadjiargyrou, M. *Biomaterials* **2003**, *24*, 4977–4985.
(21) Zeng, J.; Chen, X.; Liang, Q.; Xu, X.; Jing, X. *Macromol. Biosci.* **2004**, *4*, 1118–1125.
(22) You, Y.; Min, B.-M.; Lee, S. J.; Lee, T. S.; Park, W. H. *J. Appl. Polym. Sci.* **2005**, *95*, 193–200.
(23) Wang, Y.-X.; Robertson, J. L.; Spillman, W. B.; Claus, R. O. *Pharm. Res.* **2004**, *21*, 1362–1373.
(24) Hasirci, V.; Lewandrowski, K.; Gresser, J. D.; Wise, D. L.; Trantolo, D. J. *J. Biotechnol.* **2001**, *86*, 135–150.
(25) Ceonzo, K.; Gaynor, A.; Shaffer, L.; Kojima, K.; Vacanti, C. A.; Stahl, G. A. *Tissue Eng.* **2006**, *12*, 301–308.
(26) Tan, H. Y.; Ishii, D.; Mahara, A.; Murakami, S.; Yamaoka, T.; Sudesh, K.; Samian, R.; Fujita, M.; Maeda, M.; Iwata, T. *Biomaterials* **2008**, *29*, 1307–1317.

BM8009363